Remote Sensing of Environment 184 (2016) 539–557

Contents lists available at ScienceDirect

Remote Sensing of Environment

journal homepage: www.elsevier.com/locate/rse

Estimation of fraction of absorbed photosynthetically active radiation from multiple satellite data: Model development and validation

Xin Tao [a,*], Shunlin Liang [a,b], Tao He [a], Huiran Jin [a]

[a] Department of Geographical Sciences, University of Maryland, College Park, MD 20742, USA
[b] State Key Laboratory of Remote Sensing Science, School of Geography, Beijing Normal University, Beijing 100875, China

ARTICLE INFO

Article history:
Received 25 February 2015
Received in revised form 12 July 2016
Accepted 31 July 2016
Available online 5 August 2016

Keywords:
FAPAR
Model retrieval
Validation
MODIS
MISR
Landsat

ABSTRACT

The fraction of absorbed photosynthetically active radiation (FAPAR) is a critical input in numerous climatological and ecological models. The targeted accuracy of FAPAR products is 10%, or 0.05, for many applications. However, most of the FAPAR products in current usage have not yet fulfilled the accuracy requirement, thus requiring further improvements. In this study, a new FAPAR estimation model is developed on the basis of the radiative transfer (RT) for a horizontally homogeneous continuous canopy. The spatially explicit parameterization of leaf-scattering and soil background reflectance is derived from a 13-year Moderate Resolution Imaging Spectroradiometer (MODIS) albedo database. The new algorithm requires the input of leaf area index (LAI), which is estimated by a hybrid geometric optical-RT model suitable for both continuous and discrete vegetation canopies in this study. The model calculated radiative surface fluxes, i.e., canopy reflectance, absorption, and transmittance, are compared with the reference data from Radiation transfer Model Intercomparison (RAMI) exercise. The evaluation results show that the model estimated FAPAR has an uncertainty of 0.08 over homogeneous and heterogeneous canopies. The FAPAR estimates from the new model are intercompared with reference satellite FAPAR products and validated with ground-based measurements at the Validation of Land European Remote Sensing Instruments (VALERI) AmeriFlux experimental sites. The validation results show that the FAPAR estimates from the new model are comparable to or slightly better in performance than the MODIS and the Multi-angle Imaging SpectroRadiometer (MISR) FAPAR products when using corresponding satellite LAI product values as the input. The FAPAR estimates are further improved when using the new LAI estimates from the hybrid model as the input. The new model adequately identifies the growing seasons and produces smooth time series curves of estimated FAPAR during a specific duration. The uncertainty is reduced to 0.1 when validating with total FAPAR measurements, and 0.08 when validating with green FAPAR measurements. The improvements are apparent in grasslands and forests with an uncertainty reduction of 0.06. The regional-scale application of the presented model generates consistent FAPAR maps at spatial resolutions of 30 m, 500 m, and 1 km from the Landsat, MODIS, and MISR data, respectively.

1. Introduction

Vegetation plays a key role in the global energy balance, carbon cycle, and water budget of the Earth by controlling the exchanges between the lower atmosphere and the continental biosphere. Vegetation photosynthesis is responsible for the conversion of about 50 PgC yr^{-1} of atmospheric CO_2 into biomass, which represents about 10% of the atmospheric carbon content (Carrer et al., 2013). Land-use changes, mainly attributed to deforestation, have led to an emission level of 1.7 PgC yr^{-1} in the tropics, offsetting by a small amount of uptake of about 0.1 PgC in temperate and boreal areas—thereby producing a net source of around 1.6 PgC yr^{-1} (Houghton, 1995). One of the most important factors to monitor vegetation growth is the distribution of the fraction of absorbed photosynthetically active radiation (FAPAR) within vegetation as it constrains the photosynthesis rate through the energy absorbed by the vegetation. The FAPAR is the fraction of incoming solar radiation in the spectral range from 400 nm to 700 nm that is absorbed by plants (Chen, 1996; Liang et al., 2012; Sellers et al., 1997). As one of the 50 Essential Climate Variables (ECVs) recognized by the UN Global Climate Observing System (GCOS, 2011), FAPAR is a critical input parameter in the biogeophysical and biogeochemical processes described by numerous climatological and ecological models, such as the Community Land Model, the Community Earth System Model, and crop growth models (Bonan et al., 2002; Kaminski et al., 2012; Maselli et al., 2008; Tian et al., 2004). The Moderate Resolution Imaging Spectroradiometer (MODIS) FAPAR product (MOD15) is a critical input for MODIS evapotranspiration (MOD16), in addition to gross (GPP) and net primary production (NPP) products (MOD17) (Liang et al., 2012). A 10% increase in FAPAR would result in equal amounts of

* Corresponding author.
E-mail address: xtao@umd.edu (X. Tao).

http://dx.doi.org/10.1016/j.rse.2016.07.036
0034-4257/

GPP, NPP, and carbon sink increases. Hall et al. (2006) conducted sensitivity analysis and determined that NPP is largely driven by FAPAR in the Carnegie Ames Stanford Approach (CASA) model, with weaker effects from the lower variability of PAR and lower sensitivity to temperature and precipitation.

Despite the existence of the aforementioned numbers, the spatial distributions of carbon sources and sinks remain a core question and a subject of debate for the broad scientific community. In this regard, an improved representation of vegetation status in the ecological modeling is desirable. The reliable estimates of GPP, NPP, and carbon flux depend on high FAPAR input accuracy. An accuracy of ± 0.05, or relative accuracy of 10%, in FAPAR is considered acceptable to describe the vegetation properties precisely and can be effectively applied in agronomical and other applications (GCOS, 2011).

FAPAR can be derived from ground measurements, although the point-scale ground measurements are insufficient for regional or global coverage (Li et al., 1995). Satellite sensors efficiently acquire land surface information at regional and global scales, representing new opportunities for monitoring biophysical parameters (Asner et al., 1998). The estimation of FAPAR from optical remote sensing is based on physical models or empirical relationships (Liang, 2007). Empirical relationships between FAPAR and observations or derivatives from observations are established without knowledge of the underlying physical mechanism in the radiative transfer (RT) process. Therefore, simplicity is the primary advantage (Gobron et al., 1999). However, no unique relationship between FAPAR and the vegetation index is universally applicable to all conditions because canopy reflectance is also dependent on other factors such as geometrical measurement and spatial resolution (Asrar et al., 1992; Friedl, 1997). Moreover, the relationship between FAPAR and the vegetation index such as the normalized difference vegetation index (NDVI) is quite sensitive to the reflectance of background material (Asrar et al., 1992). Physical models analyze the interactions between solar radiation and vegetation canopies and reveal cause–effect relationships (Pinty et al., 2011; Widlowski et al., 2007). They are generally applicable to most conditions including over different land covers and during different time periods, although they require complex parameterizations. This study focuses on improving FAPAR accuracy under various conditions, and thus chooses to develop physical models.

Physical models for the retrieval of biophysical characteristics from reflected radiation of canopy can be divided into several classes (Liang, 2004): RT, geometric-optical, hybrid, and Monte Carlo, in addition to other computer simulations. The pure geometric-optical model considers only single scattering within the canopy, whereas an RT model also includes multiple scattering. Monte Carlo models and computer simulations are based on RT principles but are executed following random events rather than explicit formulae, and therefore are computationally intensive. They may be used as surrogate truths to evaluate other RT and geometric-optical models (Widlowski, 2010; Widlowski et al., 2007). An RT model is developed to calculate FAPAR in this study because of its theoretically high accuracy by including both single and multiple scattering and efficiency by following the explicit formulae.

In addition to the retrieval model performance, the determinants of FAPAR accuracy can be traced to the accuracy of such input parameter as leaf area index (LAI), soil background reflectance, and fractional canopy cover. LAI is one of the most important parameters in the determination of FAPAR, and its accuracy directly influences that of FAPAR. A 10% change in tree LAI could account for a 55% change in FAPAR (Asner et al., 1998). The collection of soil background reflectance is important for guaranteeing that the simulated reflectance can cover the entire set of observed surface reflectance data (Fang et al., 2012; Knyazikhin et al., 1998b; Shabanov et al., 2005). Otherwise, saturation of the relationship between FAPAR and surface reflectance may occur; very high FAPAR values are not reliable (Weiss et al., 2007). The correct estimation of FAPAR also relies on that of fractional canopy cover, the underestimation of which might cause unrealistically high FAPAR values (Kanniah et al., 2009). In addition to the development of new FAPAR retrieval models suitable for various land-cover types, this study also aims at improving the accuracy of FAPAR estimates by using more accurate model inputs such as LAI and soil background and leaf-scattering albedos (Xiao et al., 2015b). The LAI is calculated by using a hybrid geometric-optic RT model considering the shadowing and multiple scattering in the canopy (Tao et al., 2009; Xu et al., 2009). The soil background and leaf-scattering albedo are generated from long time series of surface anisotropy products (He et al., 2015; Tao et al., 2013). The FAPAR estimates from this study is green FAPAR considering both direct and diffuse radiation, which are validated with in-situ green and total FAPAR measurements (Tao et al., 2015).

The direct validation of satellite FAPAR products with ground measurements has generated some encouraging results, particularly when compared with previous versions of FAPAR products. The MODIS Collection 4 FAPAR product has been validated with ground measurements to demonstrate an accuracy of 0.2 (Baret et al., 2007; Fensholt et al., 2004; Huemmrich et al., 2005; Olofsson and Eklundh, 2007; Steinberg et al., 2006; Turner et al., 2005; Weiss et al., 2007; Yang et al., 2006), and the MODIS Collection 5 FAPAR product presents an improved accuracy to around 0.1 (Baret et al., 2013; Camacho et al., 2013; Martinez et al., 2013; McCallum et al., 2010; Pickett-Heaps et al., 2014; Xiao et al., 2015a). This improvement could be the result of a new stochastic RT model, which adequately captures the 3D effects of foliage clumping and species mixtures of natural ecosystems (Kanniah et al., 2009). The Multi-angle Imaging SpectroRadiometer (MISR) FAPAR product exhibits performance similar to that of the MODIS C5 FAPAR product. However, the MODIS and MISR FAPAR products might show overestimation at certain sites. For example, Martinez et al. (2013) reported that MODIS tends to provide high values in cultivated areas and Mediterranean forests, such as the Puechabon. The MODIS FAPAR product may also have positive bias for very low FAPAR values. A similar overestimation problem has been detected in MISR FAPAR data, with a positive bias as large as 0.16 in broadleaf forests (Hu et al., 2007). In addition to the overestimation problem, underestimations have been detected in the MODIS Collection 4 FAPAR product for certain sites in Switzerland (Olofsson and Eklundh, 2007). Overall, the current FAPAR products are close to, but have not fulfilled, the accuracy requirement, and further improvements are still needed (Tao et al., 2015).

This study tests how well the FAPAR accuracy can be improved from multiple satellite surface reflectance products with a new model and more accurate model inputs. Section 2 introduces data for FAPAR estimation and validation, and Section 3 describes a new model for FAPAR retrieval. The FAPAR estimates from this new model are compared with reference data and validated with in-situ measurements at the site scale in Section 4, and the model is applied to multiple resolution images at the regional scale in Section 5. Section 6 offers a discussion of the findings and conclusions.

2. Data

The data used in this study include satellite surface reflectance data, FAPAR products derived from MODIS and MISR, and FAPAR in-situ measurements from two groups of experimental sites.

2.1. Satellite surface reflectance

The MODIS, MISR, Landsat Thematic Mapper (TM), and Enhanced Thematic Mapper Plus (ETM+) reflectance data are used for FAPAR estimation. Satellite surface reflectance products for FAPAR retrieval are listed in Table 1. Different spatial resolutions of FAPAR estimates can induce the scaling effect of FAPAR, which occurs when the surface is heterogeneous and the retrieval algorithm is nonlinear (Tao et al., 2009; Xu et al., 2009). Because of the scale difference, the validation results at more homogeneous sites are expected to have a higher FAPAR accuracy. We evaluate the heterogeneity around the validation sites as described

Table 1
The characteristics of satellite surface reflectance products used in this study.

Reflectance product	Temporal coverage	Temporal resolution	Spatial resolution	Projection
MODIS MOD09 (C5) (WWW1)	Feb 18, 2000–	8 days	500 m	Sinusoidal
MISR (L2) (WWW2)	Feb 24, 2000–	Equator: 9 days, Polar: 2 days	1 km	Space Oblique Mercator
TM (WWW3)	Mar 1, 1984–	16 days	30 m	Universal Transverse Mercator (UTM)
ETM+ (WWW3)	Apr 15, 1999–	16 days	30 m	UTM

Table 2
The characteristics of moderate-resolution satellite FAPAR products used in this study.

FAPAR product	Temporal coverage	Temporal resolution	Spatial resolution	Projection	Algorithm
MODIS MOD15 (C5) (WWW1)	Feb 18, 2000–	8 days	1 km	Sinusoidal	Look up table method built on 3D stochastic radiative transfer model for different biomes (Myneni et al., 2002).
MISR (L2) (WWW2)	Feb 24, 2000–	Equator: 9 days, Polar: 2 days	1 km	Space Oblique Mercator	Radiative transfer (RT) model with inputs of LAI and soil reflectance without assumptions on biomes (Knyazikhin et al., 1998a).

in Tao et al. (2015). The FAPAR accuracy at different sites is analyzed and the impact of site heterogeneity on FAPAR accuracy is explored.

2.2. Satellite FAPAR products

The FAPAR estimates are compared with the MODIS and MISR FAPAR products (Hu et al., 2003; Knyazikhin et al., 1998a; Myneni et al., 2002). Satellite FAPAR products have certain differences in the product definitions regarding the inclusion or exclusion of diffuse radiation. The MISR FAPAR product is the total FAPAR at 10:30 am local time, considering both direct and diffuse radiation absorbed by the entire canopy. The MODIS FAPAR product considers only direct radiation, which may result in a smaller value than that of the MISR FAPAR (Hu et al., 2003; Tao et al., 2015). Regardless of the definition, differences among FAPAR products vary by land cover and are larger than expected. The poorest agreement in the FAPAR magnitude among the datasets occurs within mixed and needleleaf forests. Agreement among datasets does not imply accuracy; however, a greater number of datasets that agree over a particular area increases the likelihood that those datasets capture the variable correctly (McCallum et al., 2010).

The spatial and temporal resolutions and temporal coverage information of the satellite FAPAR products used in this paper, as well as their retrieval algorithms, are listed in Table 2. The spatial resolutions of satellite FAPAR products are both 1 km, although the temporal resolutions vary from two to nine days. The temporal values of ground-based FAPAR are aggregated to the temporal resolutions of satellite FAPAR products to validate their accuracy.

2.3. FAPAR in-situ measurements

The FAPAR validation data are derived from two groups of experimental sites: Validation of Land European Remote sensing Instruments (VALERI, WWW4) and AmeriFlux (WWW5). The VALERI sites are widely distributed around the world and useful for spatial validation over different land-cover types (Camacho et al., 2013; Weiss et al., 2007). The AmeriFlux sites are intended for the temporal validation of FAPAR estimates and products, therefore those AmeriFlux sites are selected with at least three years of ground-based continuous measurements of FAPAR. The 27 validation sites include 9 forest sites comprising 1 AmeriFlux and 8 VALERI, 12 crop sites comprising 3 AmeriFlux and 8 VALERI, 6 grass sites of VALERI, and 1 shrubland site of VALERI. Their distributions are shown in Fig. 1.

Four components are measured to compute FAPAR at AmeriFlux sites, including incoming and outgoing solar flux and flux from and to the ground. Incoming (outgoing) solar flux is measured with Li-Cor point quantum sensors aimed upward (downward), and placed at approximately 6 m above the ground. Flux transmitted through the canopy to the ground is measured with Li-Cor line quantum sensors placed at approximately 2 cm above the ground, pointing upward. Flux reflected by the ground was measured with Li-Cor line quantum sensors placed approximately 12 cm above the ground, pointing downward (Hanan et al., 2002). Hourly FAPAR is calculated as the ratio of absorbed photosynthetically active radiation and incoming solar flux. All the daytime radiation values were computed by integrating the hourly measurements during a day when incoming solar flux exceeded 1 μmol/m^2/s, and daily FAPAR was then calculated. Digital hemispherical photos are used to calculate FAPAR at VALERI sites, which corresponds to the fraction of intercepted PAR. High spatial resolution remote sensing data are used as a bridge to obtain the FAPAR values in the medium resolution pixels. The differences in the interception and absorptions are small (<5%), which are considered by adding error bars on the in-situ data in this study (Serbin et al., 2013).

3. Methodology

In moderate-resolution images, vegetation pixels are almost continuously distributed across large regions. Therefore, we assume that the land cover is horizontally homogeneous within the targeted surface, and we develop a four-stream RT model of continuous canopy for FAPAR retrieval. Canopy absorptance along the direct- and diffuse-light penetrating paths are calculated separately and summed by using a ratio of scattering light. We denote T_0, T_f, and T_v as the canopy transmittance along the direct-light penetrating, the diffuse-light penetrating, and the observing paths, respectively, and $\rho_{v,\lambda}$, $\rho_{g,\lambda}$, and $\rho_{c,\lambda}$ as the hemispherical albedos of vegetation, soil background, and leaf, respectively. FAPAR is calculated as the integral of canopy absorptance in the upper hemisphere from 400 nm to 700 nm, in the following manner:

$$\begin{aligned}\mathrm{FAPAR} = (1-\beta)\int_{400}^{700}\int_{0}^{\frac{\pi}{2}}\left[\left(1-T_0-2\rho_{v,\lambda}(\theta)\right)+\left(1-T_v(\theta)-2\rho_{v,\lambda}(\theta)\right)\frac{T_0\rho_{g,\lambda}}{1-\rho_{g,\lambda}\rho_{v,\lambda}(\theta)}\right]\cos\theta\sin\theta d\theta d\lambda \\ +\beta\int_{400}^{700}\int_{0}^{\frac{\pi}{2}}\left[\left(1-T_f-2\rho_{v,\lambda}(\theta)\right)+\left(1-T_v(\theta)-2\rho_{v,\lambda}(\theta)\right)\frac{T_f\rho_{g,\lambda}}{1-\rho_{g,\lambda}\rho_{v,\lambda}(\theta)}\right]\cos\theta\sin\theta d\theta d\lambda\end{aligned} \quad (1)$$

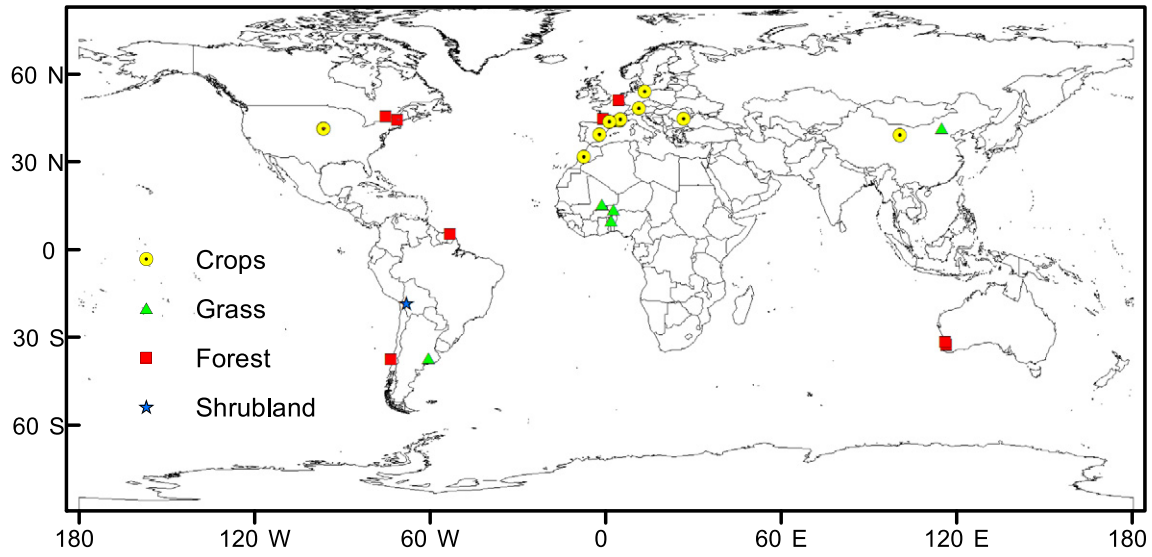

Fig. 1. The distributions of the 27 validation sites. The four AmeriFlux sites in the United States are covered in the two study regions in Section 5. Three AmeriFlux and three VALERI sites are close to each other, which may not be distinguishable at the global scale here.

where the canopy transmittance along the direct-light penetrating, the diffuse-light penetrating, and the observing paths is:

$$T_{0,f,v} = \exp\left(-\lambda_0 \frac{G_{s,f,v}}{\mu_{s,f,v}} LAI\right) \tag{2}$$

and hemispherical albedo of vegetation is:

$$\rho_{v,\lambda}(\theta) = \rho_{c,\lambda}\left[1-\exp\left(-\lambda_0 \frac{G_v}{\mu_v(\theta)} \Gamma(\phi) LAI\right)\right] + \beta\rho_{c,\lambda}\left[\exp\left(-\lambda_0 \frac{G_v}{\mu_v(\theta)} \Gamma(\phi) LAI\right) - \exp\left(-\lambda_0 \frac{G_v}{\mu_v(\theta)} LAI\right)\right] \tag{3}$$

In Eqs. (2) and (3), λ_0 is a Nilson parameter accounting for the vegetation clumping effect; μ_s and $\mu_v(\theta)$ are the cosine values of solar (θ_s) and viewing (θ) zenith angles, respectively; β is the ratio of scattering light; and G_s and G_v are the mean projections of a unit foliage area along the solar and viewing directions, respectively (Liang, 2004; Ross, 1981):

$$G_{s,v} = \frac{1}{2\pi}\int_{2\pi} g_L(\Omega_L)\left|\Omega_L \cdot \Omega_{s,v}\right| d\Omega_L \tag{4}$$

where $1/2\pi \cdot g_L(\Omega_L)$ is the probability density of a distribution of leaf normals with respect to the upper hemisphere, i.e., leaf-angle distribution.

An empirical function $\Gamma(\phi)$ in Eq. (3) describes the hot-spot phenomenon, where ϕ accounts for sun–target–sensor position and depends on the angle between solar and viewing directions and the leaf-angle distribution of the canopy.

$$\Gamma(\phi) = \exp\left(\frac{-\phi}{180-\phi}\right) \tag{5}$$

The LAI is assumed known for FAPAR estimation, as a hybrid geometric optic-radiative transfer model for LAI retrieval has been previously developed and is included in the Appendix for convenience (Tao et al., 2009; Xu et al., 2009).

Other important inputs for FAPAR estimation proposed in this study are soil background and leaf-scattering albedos. Certain typical soil background and leaf-scattering albedos could be used for simplicity, but they may deviate from local conditions. Considering the applicability of surface albedos at local conditions, we establish a database of soil background and leaf-scattering albedos upon 13 years of surface albedo time series (He et al., 2015; Tao et al., 2013). The multi-year mean soil background and leaf-scattering albedo were generated by using the 500 m spatial resolution MODIS surface anisotropy products (MCD43A) during the period 2000–2012. The soil-line characteristics are used to separate vegetation and bare soil on a pixel basis over the United States. The leaf-scattering albedo is generated from the vegetation albedo at the peak of the growing season. Therefore, the database provides local pixel-based soil background and leaf-scattering albedos as inputs for FAPAR estimation models. The component albedos can be used to derive biophysical variables such as LAI, FAPAR, GPP, and they also serve as inputs in land surface models to characterize surface energy budget. Fig. 2 shows examples of the derived soil background and leaf-scattering albedos.

Overall, the FAPAR estimation model described in Eqs. (1)–(5) accounts for reflective anisotropic characteristics caused by sun–target–sensor geometry, the vegetation clumping effect, and the hot-spot effect. In consideration of model simplicity and computational efficiency, it neglects reflective anisotropic characteristics caused by leaf and soil background. The parameters of the new FAPAR model are LAI, λ_0, G, $\rho_{c,\lambda}$, $\rho_{g,\lambda}$, and θ_s. The LAI is calculated from a hybrid geometric optic-radiative transfer model, θ_s is extracted from satellite data, and the other parameters (λ_0, G, $\rho_{c,\lambda}$, and $\rho_{g,\lambda}$) are from prior knowledge or locally applicable database. For simplicity, the model is referred to as the 4S model hereafter. The FAPAR estimated from

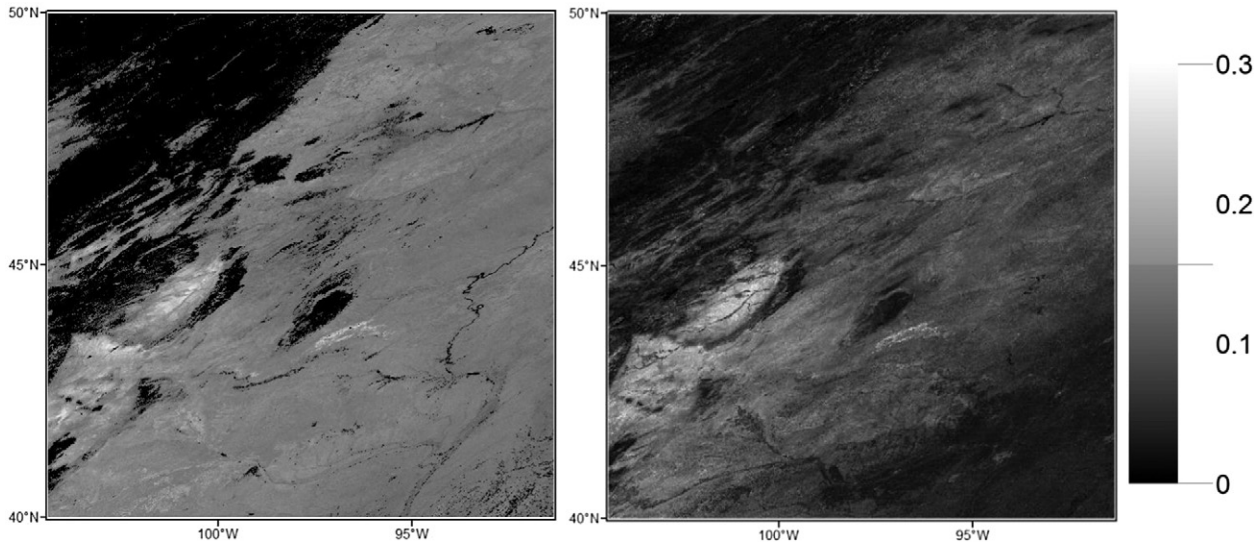

Fig. 2. The soil background (left) and leaf-scattering (right) albedos at the red band on clear days in a 13-year surface albedo database within the extent of a MODIS tile H10V04.

the model is green FAPAR considering both direct and diffuse radiation. Most of the current FAPAR products do not consider absorption by diffuse radiation, and no official green FAPAR product including both direct and diffuse radiation is available this far (Tao et al., 2015). Therefore, this study serves as a good complement to the current FAPAR products.

4. Validation and comparison with reference data

4.1. Comparison with the RAMI reference data

The model is used to simulate the spectral characteristics of the scenes in the fourth phase of the Radiation transfer Model Intercomparison (RAMI) exercise in the Project for Intercomparison of Land-Surface Parameterizations (PILPS). The RAMI4PILPS suite of experiments includes structurally homogeneous test cases (grassland and closed forest) and heterogeneous test cases (open forest and shrubland). The architecture, spectral properties and illumination conditions of the canopy are described in each case. The participants are required to deliver three radiative surface fluxes: canopy reflectance, absorption, and transmittance. The results are evaluated by the reference data from the three-dimensional Monte Carlo model, raytran (Govaerts and Verstraete, 1998). More details of the experiments are available in Widlowski et al. (2011; 2008) and WWW6.

The comparisons between the model calculated radiative surface fluxes and the reference data are shown in Fig. 3. The model simulated reflectance, transmittance, and absorption agree well with the reference data. The R^2 is above 0.91, the root mean square error (RMSE) is around 0.07, and the bias is <0.06. The comparison results prove the feasibility of the model to simulate canopy spectral characteristics accurately.

More specifically, the model simulated reflectance, transmittance, and absorption in the near infrared band agree well with the reference data of RAMI (Fig. 4). The R^2 is around 0.85, RMSE is around 0.07, and the bias is around 0.04. The comparisons of the radiative surface fluxes in the visible band are shown in Fig. 5. The R^2 is above 0.93, RMSE is around 0.05, and the bias is around 0.03. The comparison results further prove the feasibility of the model to simulate canopy spectral characteristics in the NIR and visible bands accurately. Compared with the statistics in the NIR band, higher accuracy of simulated radiative surface fluxes is obtained in the visible band. The RAMI experiment shows that the modeled FAPAR has an uncertainty of 0.076 and a slight underestimation of 0.046.

The mean of the absolute values of the deviations from the reference data in homogeneous and heterogeneous canopies in the visible and NIR domain is provided in Table 3. The standard deviations of the absolute values of the deviations are included in the table as well. The model shows a better performance over homogeneous vegetation canopies than over heterogeneous vegetation canopies in the visible band. However, the model has a better performance over heterogeneous

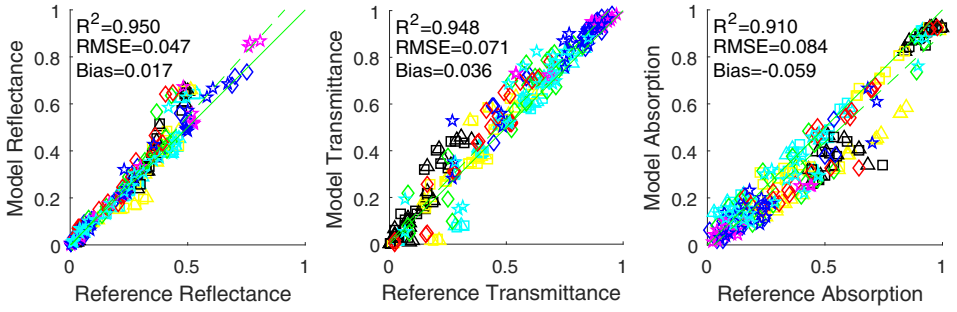

Fig. 3. Scatterplots of canopy reflectance, transmittance, and absorption between the model and the RAMI reference data for the four vegetation types: grassland (△), closed forest (□), open forest (◇), and shrubland (*). The canopy with LAI of 0.25 is displayed in magenta, 0.5 in blue, 1 in cyan, 1.5 in green, 2 in yellow, 2.5 in red, and 4 in black, respectively.

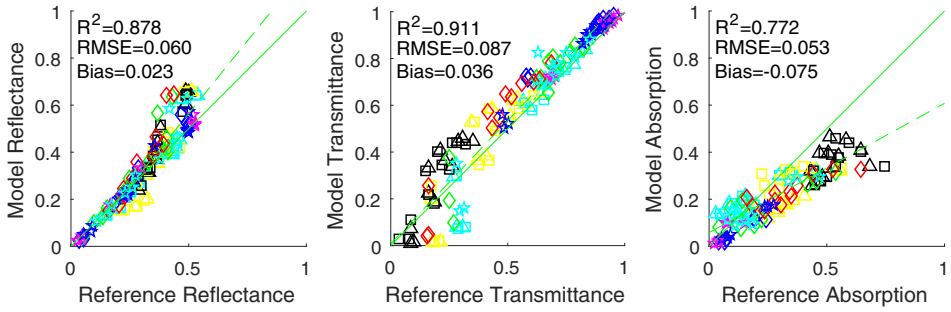

Fig. 4. Scatterplots of canopy reflectance, transmittance, and absorption in the near infrared band between the model and the RAMI reference data for the four vegetation types: grassland (△), closed forest (□), open forest (◇), and shrubland (*). The canopy with LAI of 0.25 is displayed in magenta, 0.5 in blue, 1 in cyan, 1.5 in green, 2 in yellow, 2.5 in red, and 4 in black, respectively.

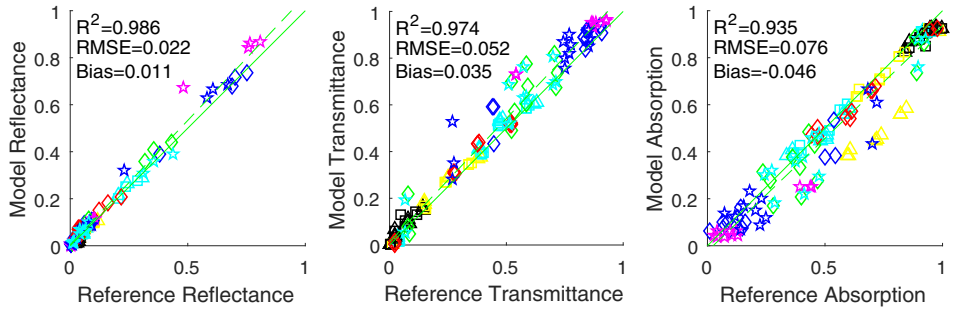

Fig. 5. Scatterplots of canopy reflectance, transmittance, and absorption in the visible band between the model and the RAMI reference data for the four vegetation types: grassland (△), closed forest (□), open forest (◇), and shrubland (*). The canopy with LAI of 0.25 is displayed in magenta, 0.5 in blue, 1 in cyan, 1.5 in green, 2 in yellow, 2.5 in red, and 4 in black, respectively.

vegetation canopies than over homogeneous vegetation canopies in the NIR band. This study focuses on estimating FAPAR in the visible band. The statistics shows that the modeled FAPAR has an average error of 0.059 over homogeneous and heterogeneous vegetation canopies.

4.2. Validation and comparison with the MODIS official FAPAR product

The near infrared and visible bands of the NASA MODIS surface reflectance data (MOD09) are used to estimate vegetation LAI, and the visible bands are used to estimate FAPAR by using the presented model. The model calculated FAPAR are validated with ground-based measurements and compared with the MODIS FAPAR products in this subsection. The quality flags are used to select high-quality MODIS data with main algorithm retrievals. As control experiments, the FAPAR is estimated directly from the MODIS surface reflectance data (referred to as MOD_4SH-based FAPAR) or from the MODIS official LAI product (referred to as MOD_4SO-based FAPAR). The FAPAR estimates by the presented model are compared with the MODIS FAPAR product and validated against 3 years of ground-based continuous measurements of FAPAR at 4 AmeriFlux sites (Fig. 6). The homogeneity index is higher at the Bartlett experimental deciduous broadleaf forest and Mead Irrigated crop sites than that at the Mead Rainfed crop site (Tao et al., 2015). Therefore, both FAPAR products and estimates from this study have a higher validation accuracy at the Bartlett site, followed by that at the Mead Irrigated sites, and the Mead Rainfed site. Compared with the MODIS FAPAR product, the FAPAR estimated from the presented model has an increased R^2 for all of the four sites (Table 4). The improvement is most obvious at the Mead Irrigated Rotation and Bartlett sites, where the R^2 is improved by around 20%. Because the model presented in this study is suitable for homogenous landscape, more significant improvements are expected at these sites.

Compared with the MOD_4SO-based FAPAR from the control experiment, the MOD_4SH based-FAPAR has similar RMSE although the R^2 is improved by about 8% on average. The FAPAR measurements at Mead Irrigated, Mead Irrigated Rotation, and Mead Rainfed sites reach zero before early April and after mid-November, which is a result of crop harvesting at those locations. The values of the MODIS FAPAR product at the three Mead sites are larger zero at the beginning and the end of the year, which could be caused by the heterogeneous land cover inside the 1×1 km extent of the MODIS FAPAR pixel. The FAPAR estimated from the MODIS official LAI product (MOD_4SO-based FAPAR) are similar to the MODIS FAPAR product, with a smooth curve over the years. The MOD_4SH-based FAPAR are derived from the model using surface reflectance data at the 500 m spatial resolution. Combined with locally

Table 3
Average values of the absolute model-to-reference difference, expressed in percent for the model simulated canopy absorption, reflectance, and transmittance in the visible and near-infrared domains for homogeneous and heterogeneous vegetation canopies.

Band	Homogeneous vegetation canopies			Heterogeneous vegetation canopies		
	Absorption	Reflectance	Transmittance	Absorption	Reflectance	Transmittance
Visible	5.30 ± 7.60	0.93 ± 0.79	1.94 ± 1.76	6.43 ± 5.97	2.00 ± 3.02	6.46 ± 6.05
NIR	10.83 ± 8.22	5.83 ± 5.34	8.26 ± 6.95	7.90 ± 6.07	3.45 ± 5.30	6.77 ± 4.47
Both	8.03 ± 8.36	3.38 ± 4.53	5.10 ± 5.96	7.05 ± 6.03	2.72 ± 4.36	6.61 ± 5.30

applicable soil background albedo data, the model can detect vegetation growing season well and reduce the FAPAR uncertainty by 5%. The improvement of the MOD_4SH-based FAPAR over the MOD_4SO-based FAPAR results from the use of improved LAI values as model input. The performance of the presented model is comparable to that of the MODIS FAPAR model when using the same LAI value as input.

The MOD_4SH-based FAPAR agrees well with in-situ measurements obtained during the first halves of the years. However, some

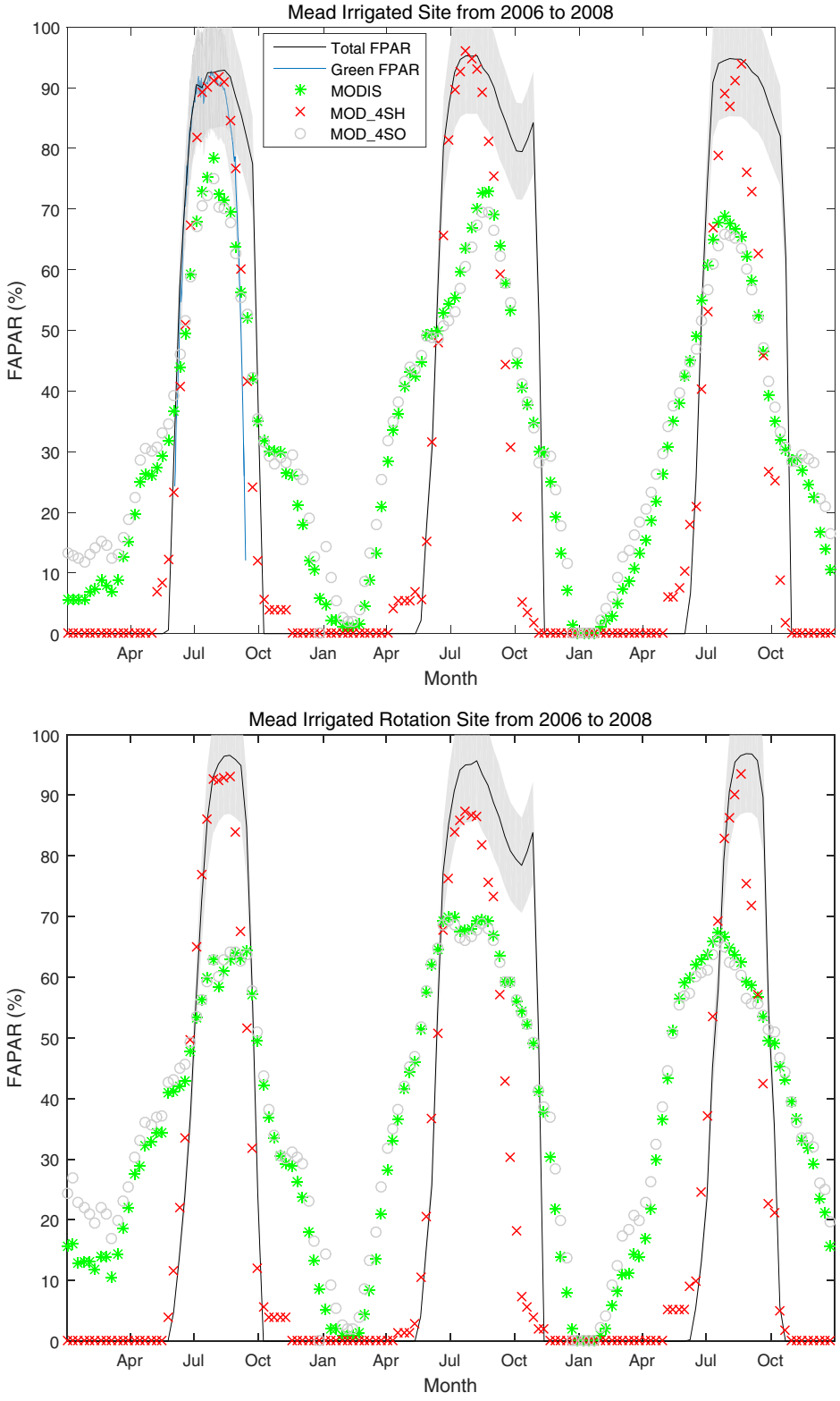

Fig. 6. The time series of in-situ FAPAR measurements and the MODIS FAPAR estimates at four AmeriFlux sites. Green FAPAR measurements are depicted in blue line in the first panel, and total FAPAR measurements are depicted in black line in all panels. The shaded area is the 10% accuracy requirement. The MODIS official FAPAR product, the FAPAR estimates using the MODIS official LAI product and the presented model, and the FAPAR estimates using the newly estimated LAI are depicted in asterisks, circles, and crosses, respectively.

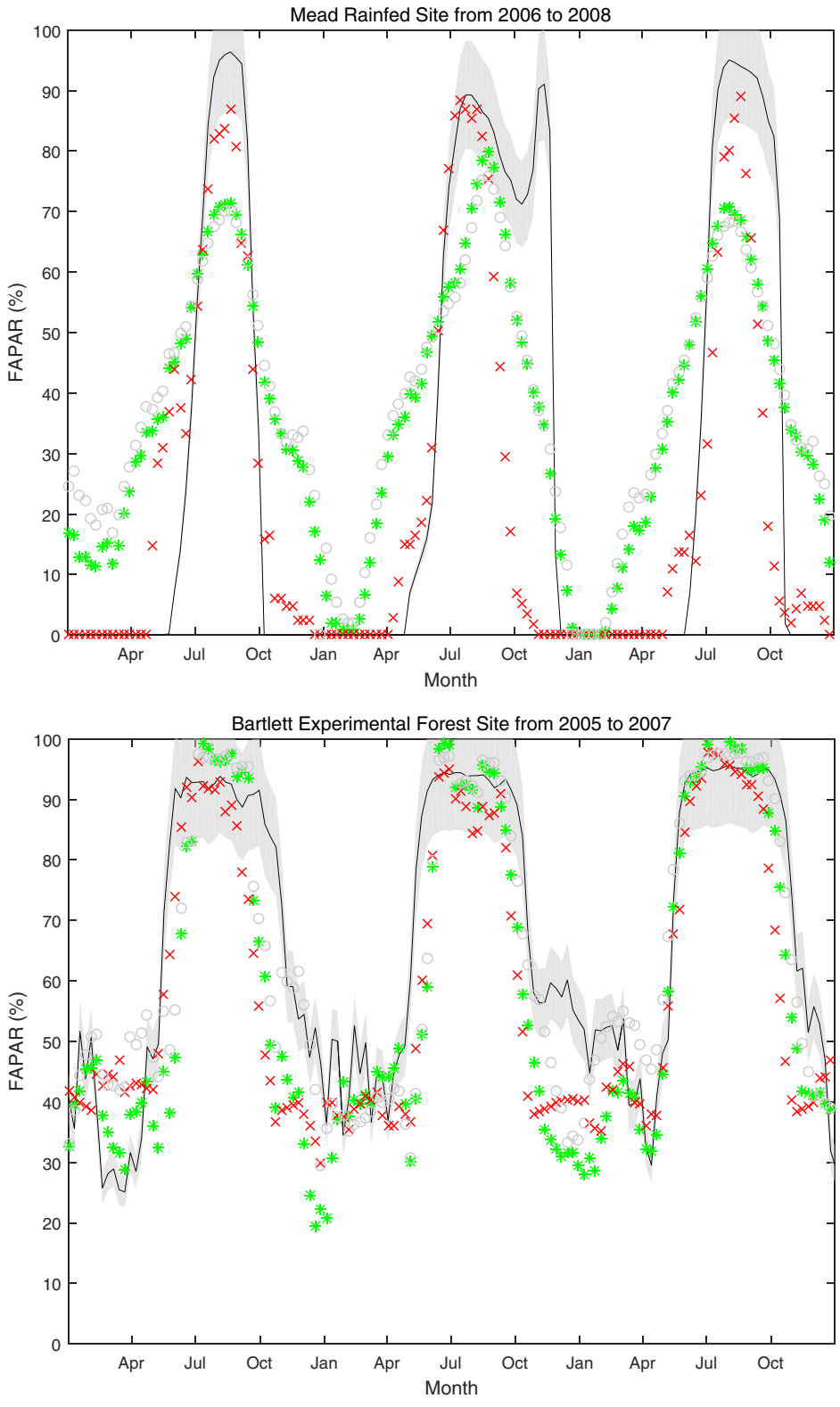

Fig. 6 (*continued*).

underestimation occurred in the FAPAR estimates at three crop sites in the latter halves of the years, specifically at the end of the growing season. This result is caused by the senescence and yellow alteration of the leaves; thus, the FAPAR from remote sensing (green FAPAR) differs from the measurements (total FAPAR) (Vina and Gitelson, 2005; Zhang et al., 2005). The FAPAR estimates from this study and the MODIS FAPAR products are lower than the ground-based measurements at the end of the growing season at the Bartlett forest site. This is because in-situ measured FAPAR includes the absorption of tree trunks and branches, which dominates total absorption, particularly at the end of the growing

Table 4
Statistics of comparisons between ground-based and space products and the estimates from this study.

Site	FAPAR	Regression equation	RMSE	Bias	R^2
Mead Irrigated	MODIS official product	$y = 0.476\,x + 0.175$	0.140	0.009	0.667
	MISR official product	$y = 0.600\,x + 0.251$	0.153	0.072	0.756
	MOD_4SO based	$y = 0.416\,x + 0.209$	0.116	0.024	0.687
	MIS_4SO based	$y = 0.588\,x + 0.320$	0.136	0.135	0.789
	MOD_4SH based	$y = 0.717\,x + 0.007$	0.139	−0.083	0.773
	MIS_4SH based	$y = 0.832\,x + 0.062$	0.132	−0.012	0.889
	Landsat_4SH based	$y = 0.764\,x - 0.010$	0.224	−0.087	0.692
Mead Irrigated Rotation	MODIS official product	$y = 0.454\,x + 0.244$	0.161	0.098	0.546
	MISR official product	$y = 0.598\,x + 0.271$	0.157	0.104	0.732
	MOD_4SO based	$y = 0.401\,x + 0.277$	0.136	0.116	0.569
	MIS_4SO based	$y = 0.533\,x + 0.278$	0.139	0.083	0.736
	MOD_4SH based	$y = 0.749\,x + 0.016$	0.141	−0.051	0.809
	MIS_4SH based	$y = 0.772\,x + 0.129$	0.181	0.034	0.774
	Landsat_4SH based	$y = 0.854\,x - 0.021$	0.170	−0.053	0.823
Mead Rainfed	MODIS official product	$y = 0.482\,x + 0.222$	0.143	0.070	0.626
	MISR official product	$y = 0.512\,x + 0.267$	0.163	0.047	0.622
	MOD_4SO based	$y = 0.418\,x + 0.258$	0.127	0.086	0.625
	MIS_4SO based	$y = 0.482\,x + 0.341$	0.149	0.107	0.637
	MOD_4SH based	$y = 0.611\,x + 0.046$	0.107	−0.069	0.632
	MIS_4SH based	$y = 0.865\,x + 0.073$	0.106	0.012	0.918
	Landsat_4SH based	$y = 0.855\,x - 0.022$	0.217	−0.053	0.731
Bartlett	MODIS official product	$y = 0.969\,x - 0.064$	0.203	−0.089	0.566
	MISR official product	$y = 1.188\,x - 0.198$	0.125	−0.086	0.842
	MOD_4SO based	$y = 0.833\,x + 0.079$	0.122	−0.033	0.729
	MIS_4SO based	$y = 0.987\,x - 0.068$	0.097	−0.076	0.858
	MOD_4SH based	$y = 0.808\,x + 0.040$	0.124	−0.089	0.709
	MIS_4SH based	$y = 0.929\,x - 0.041$	0.085	−0.083	0.898
	Landsat_4SH based	$y = 1.322\,x - 0.340$	0.133	−0.078	0.790

MOD_4SO based: the FAPAR estimates using MODIS official LAI product and the presented model.
MIS_4SO based: the FAPAR estimates using MISR official LAI product and the presented model.
MOD_4SH based: the FAPAR estimates using MODIS surface reflectance data and the presented model.
MIS_4SH based: the FAPAR estimates using MISR surface reflectance data and the presented model.
Landsat_4SH based: the FAPAR estimates using Landsat surface reflectance data and the presented model.

season when leaf coverage is absent (Fang et al., 2005). Consequently, the validation accuracy of the MODIS FAPAR product is improved from 0.140 to 0.082 and that of MOD_4SH-based FAPAR is improved from 0.139 to 0.069 when using green FAPAR measurements as validation data. However, the calculation of green FAPAR requires additional simultaneous measurements of green LAI and total LAI to distinguish between green leaves and yellow leaves. The process is labor extensive, and thus green FAPAR measurements are not collected for all the years. Therefore, total FAPAR measurements are used as the main validation data in this study, considering its temporal continuity.

The MODIS FAPAR product and the FAPAR estimates from this study are validated with ground measurements of VALERI. The results are shown in Fig. 7. Overall, the MOD_4SO-based FAPAR has slightly increased R^2 and decreased RMSE compared with the MODIS FAPAR product. Both the MODIS FAPAR product and MOD_4SH-based FAPAR have little bias (<0.02) compared with in-situ data; however, the FAPAR estimates from this study have better correlation with in-situ data and smaller RMSE than the MODIS FAPAR product. The improvements of the MOD_4SH-based FAPAR over the MOD_4SO-based FAPAR are attributed to the improved LAI values as input. The MODIS FAPAR product performs well at shrubland and crop sites; however, the deviations from in-situ values are large at forest and grass sites. The FAPAR estimates from this study reduced the uncertainty at forest and grass sites from 0.155 to 0.094. The FAPAR estimates and products are lower than ground-based measurements at some forest sites. This is because in-situ measurements of FAPAR include the absorption of tree trunks and branches, while remotely sensed FAPAR is mainly related to that of green leaves.

4.3. Validation and comparison with the MISR official FAPAR product

The MISR surface directional reflectance data are used to estimate vegetation LAI and FAPAR values using the presented model. Moreover, the FAPAR estimates are compared with the MISR FAPAR

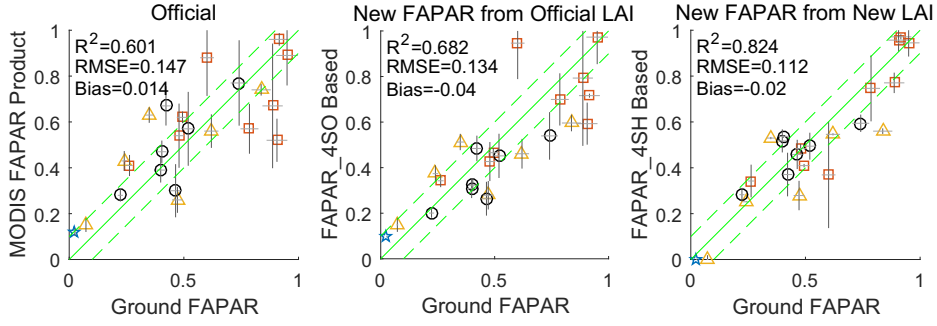

Fig. 7. Validation of the FAPAR estimates from this study and the MODIS official FAPAR product by using in-situ measurements at VALERI sites. The land cover of shrubland is displayed by a pentagram (*), grass by triangle (Δ), forest by square (□), and crops by circle (○). Horizontal and vertical bars correspond to the uncertainties (±σ). The middle line is $y = x$. The other lines are $y = x \pm 0.1$, respectively.

product. In the control experiments, the FAPAR is estimated directly from the MISR surface directional reflectance data (referred to as MIS_4SH-based FAPAR) or from the MISR official LAI product (referred to as MIS_4SO-based FAPAR). The FAPAR estimates are validated against 3 years of continuous measurements at 4 AmeriFlux sites (Fig. 8). Compared with the MODIS FAPAR product in Fig. 6,

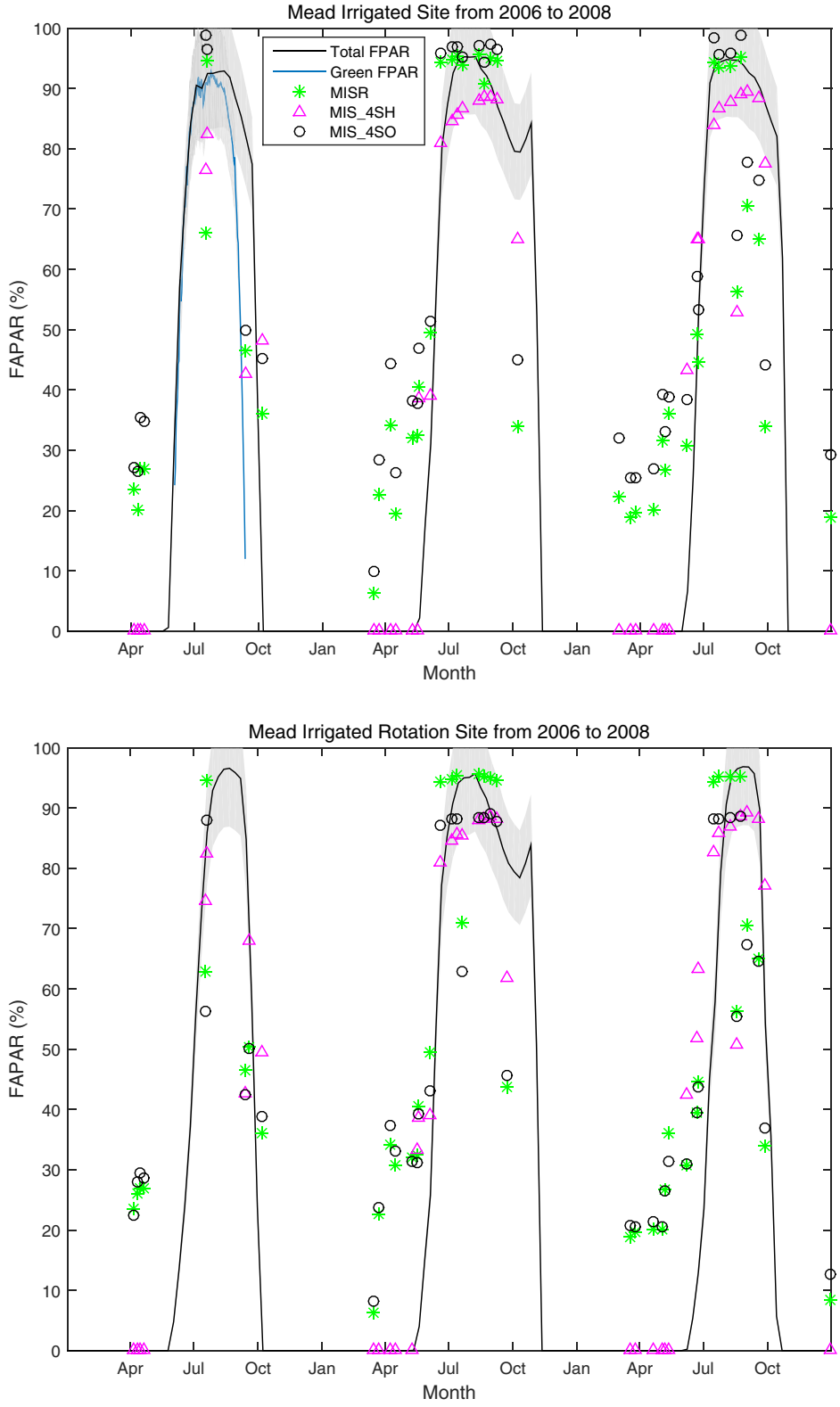

Fig. 8. The time series of in-situ FAPAR measurements and the MISR FAPAR estimates at four AmeriFlux sites. Green FAPAR measurements are depicted in blue line in the first panel, and total FAPAR measurements are depicted in black line in all panels. The shaded area is the 10% accuracy requirement. The MISR official FAPAR product, the FAPAR estimates using the MISR official LAI product and the presented model, and the FAPAR estimates using the newly estimated LAI are depicted in asterisks, circles, and diamonds, respectively.

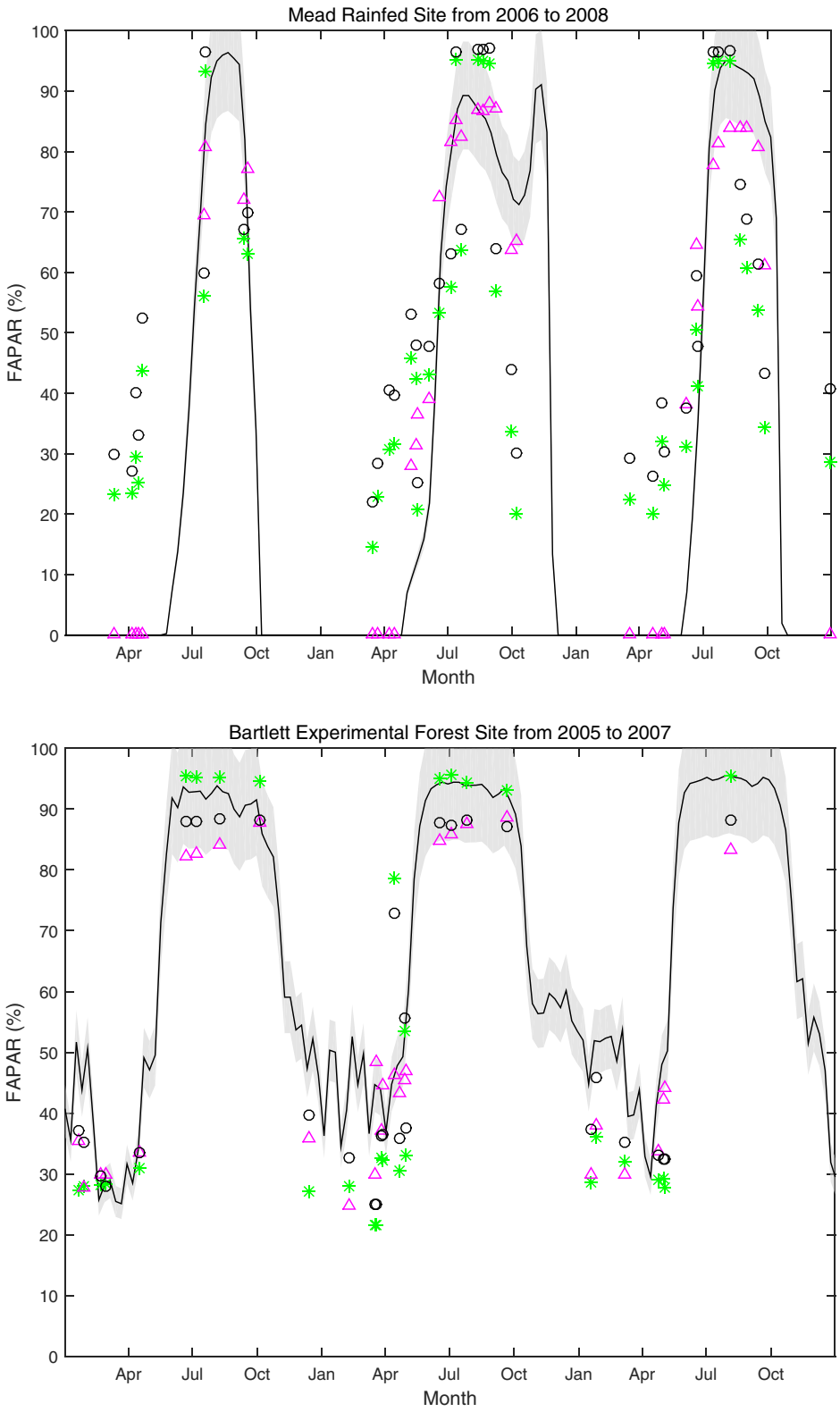

Fig. 8 (*continued*).

the MISR FAPAR product and the FAPAR estimates from this study have higher values, particularly in the middle of the vegetation growing season. The MIS_4SO-based FAPAR is similar to the MISR FAPAR product, showing a smooth trend over the years. Compared with the MISR FAPAR product, the FAPAR estimates by the presented model have increased R^2 for all four sites (Table 4). The improvement is most obvious at the Bartlett Experimental forest site and Mead Rainfed sites, with a reduction of RMSE by around 0.05. The improvement of the MIS_4SH-based FAPAR over the MIS_4SO-based FAPAR is also a result of using improved LAI values as input. The performance

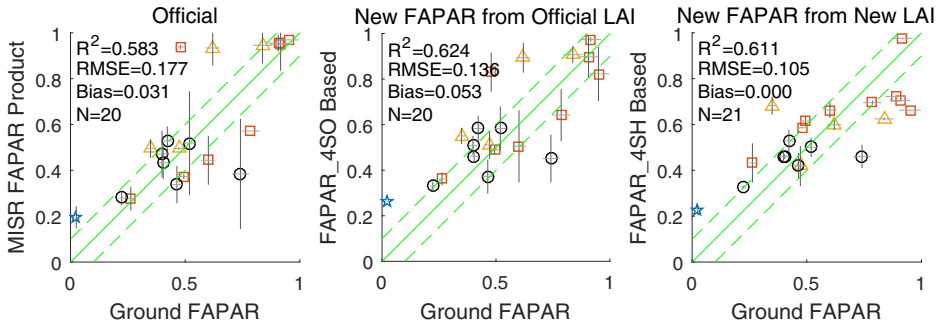

Fig. 9. Validation of the FAPAR estimates from this study and the MISR official FAPAR products by using in-situ measurements at VALERI sites. The land cover of shrubland is displayed by a pentagram (*), grass by triangle (△), forest by square (□), and crops by circle (○). Horizontal and vertical bars correspond to the uncertainties (±σ). The middle line is $y = x$. The other lines are $y = x \pm 0.1$, respectively.

of the presented model is comparable to that of the MISR FAPAR model when using the same LAI value as input.

The MISR FAPAR product and the FAPAR estimates from MISR reflectance data by the presented model are validated at the VALERI sites, as shown in Fig. 9. The MIS_4SO-based FAPAR has improved R^2 and reduced RMSE values compared with the MISR FAPAR product. Both the MISR FAPAR product and the MIS_4SH-based FAPAR have little positive to almost no bias (<0.035) compared with in-situ data, although the latter has better correlation with in-situ data and smaller RSME than the former. The improvement of the MIS_4SH over the MIS_4SO indicates that the improvement of the FAPAR estimates is also a result of improved LAI values as input. It should be noted that the RMSE of the MISR FAPAR estimates, at 0.105, is slightly smaller than that of the MODIS FAPAR estimates from this study, at 0.112. Both the MODIS and the MISR FAPAR estimates from this study performed well at grass and forest sites with an average accuracy of 0.104. The MISR FAPAR estimates are improved at crop sites compared with the corresponding MODIS FAPAR estimates.

4.4. Validation of the FAPAR estimates from Landsat data

The Landsat surface reflectance data are used to estimate vegetation FAPAR, which are then validated with the in-situ measured FAPAR at four AmeriFlux sites, as shown in Fig. 10. The statistics of comparisons between the ground-based and Landsat FAPAR estimates are listed in Table 4. The Landsat FAPAR estimates have good performance at the Mead Irrigated Rotation and the Bartlett sites, and performance comparable to the MODIS and MISR FAPAR products and the MODIS and MISR FAPAR estimates of this study at the Mead Irrigated and Mead Rainfed sites. The overall R^2 at these sites is 0.76, and the bias is small, proving the feasibility of the proposed method being applied to high-resolution data.

The LAI and FAPAR estimated from the Landsat data are compared with the in-situ measured FAPAR at VALERI sites, as shown in Fig. 11. Both the LAI and FAPAR estimates have little positive bias (<0.045) compared with in-situ data. The FAPAR estimates have a very low RMSE and high correlation with in-situ data. Overall, the performance of the FAPAR estimates is better than that of the LAI estimates possibly because of the smaller range of FAPAR values than that of the LAI values. Similarly, better performances are observed in the MODIS and MISR FAPAR products than in the LAI products. The Landsat FAPAR estimates from this study perform well for grass, forest, and shrubland land-cover types, but are not as good as the MODIS and the MISR FAPAR estimates at crop sites. This could be caused by the large uncertainty of the clumping index in the model over crops, which could be more heterogeneous than other land covers due to the existence of row crops. The Landsat FAPAR values are missing or invalid at five sites; thus, the retrieval rate of the Landsat FAPAR estimates is lower than that of MISR and MODIS. Overall, improvements are noted when using high-resolution data, although some uncertainty is introduced by using soil/leaf albedos from another sensor and by cloud contamination of the Landsat data.

5. Application at the regional scale

The FAPAR estimation results are validated at the site scale, and the method is applied further at the regional scale. Multiple satellite data with different spatial resolutions are used to estimate the FAPAR values for analysis across scales. Two study regions covering the four AmeriFlux sites in the United States are selected (Fig. 1). The MODIS tiles and the MISR and Landsat orbits covering the two study regions are listed in Table 5. The temporal resolutions of the MISR, MODIS, and Landsat TM/ETM + reflectance or FAPAR products are 2–9 days, 8 days, and 16 days, respectively. The MISR, MODIS, and Landsat scenes around the four AmeriFlux sites in the vegetation growing season are carefully selected to have close imaging dates as well as high-quality data without cloud contamination. The imaging dates of the products in each case differ within four days (Table 5). We assume that the vegetation remains unchanged within such a short period; therefore, the intercomparison of FAPAR among different sensors is reliable.

The Landsat reflectance data are atmospherically corrected by using the Landsat Ecosystem Disturbance Adaptive Processing System (LEDAPS) preprocessing code (Masek et al., 2006). The missing scan lines in the ETM + image are filled with values of nearest pixels. The Landsat TM and ETM + surface reflectance scenes are used for estimating FAPAR at a spatial resolution of 30 m. The MISR and MODIS surface reflectance products (MISR L2 and MOD09) are directly used for estimating FAPAR at spatial resolutions of 1 km and 500 m. The MISR and the MODIS FAPAR products (MISR L2 and MOD15) are intended for intercomparison with the FAPAR estimates from this study.

The MODIS FAPAR product uses MCD12 land cover product to distinguish 13 land covers globally. The National Land Cover Database 2006 (NLCD 2006) uses a 16-class land cover classification scheme for Landsat images. A combined land cover classification scheme of the two is used here considering the existing land cover types in the two study regions. Consequently, the MISR, MODIS, and Landsat images are classified into evergreen forest, deciduous forest, urban, grass, crops, barren soil, and water body. The presented model is applied on the surface reflectance and the classified images to estimate the vegetation LAI and FAPAR values. The distributions of the FAPAR estimates from the MISR, MODIS, and Landsat images in Case 1 are shown in Fig. 12(a)–(c), respectively. For comparison, the MISR and the MODIS FAPAR products are shown in Fig. 12(d)–(e), respectively. The distributions of the FAPAR estimates in Case 2 are shown in Fig. 13(a)–(c). For comparison, the MISR and the MODIS FAPAR products are shown in Fig. 13(d)–(e), respectively. The MISR FAPAR product is consistently

higher (>0.15) than the MODIS FPAR product in Case 1, and the MODIS and the MISR FAPAR products agree well in Case 2. However, the FAPAR estimates from this study are consistent across different scales in both cases. The values have similar distribution patterns across scales, in which the highest values are observed in evergreen forests, followed by deciduous forests, crops; and rivers and central urban areas, where the FAPAR estimates are close to zero.

The frequency histograms of the MODIS and the MISR FAPAR products are shown in red and blue bars in Fig. 14(b) and (d) for Cases 1 and 2, respectively. The MISR FAPAR product has a larger mean (by

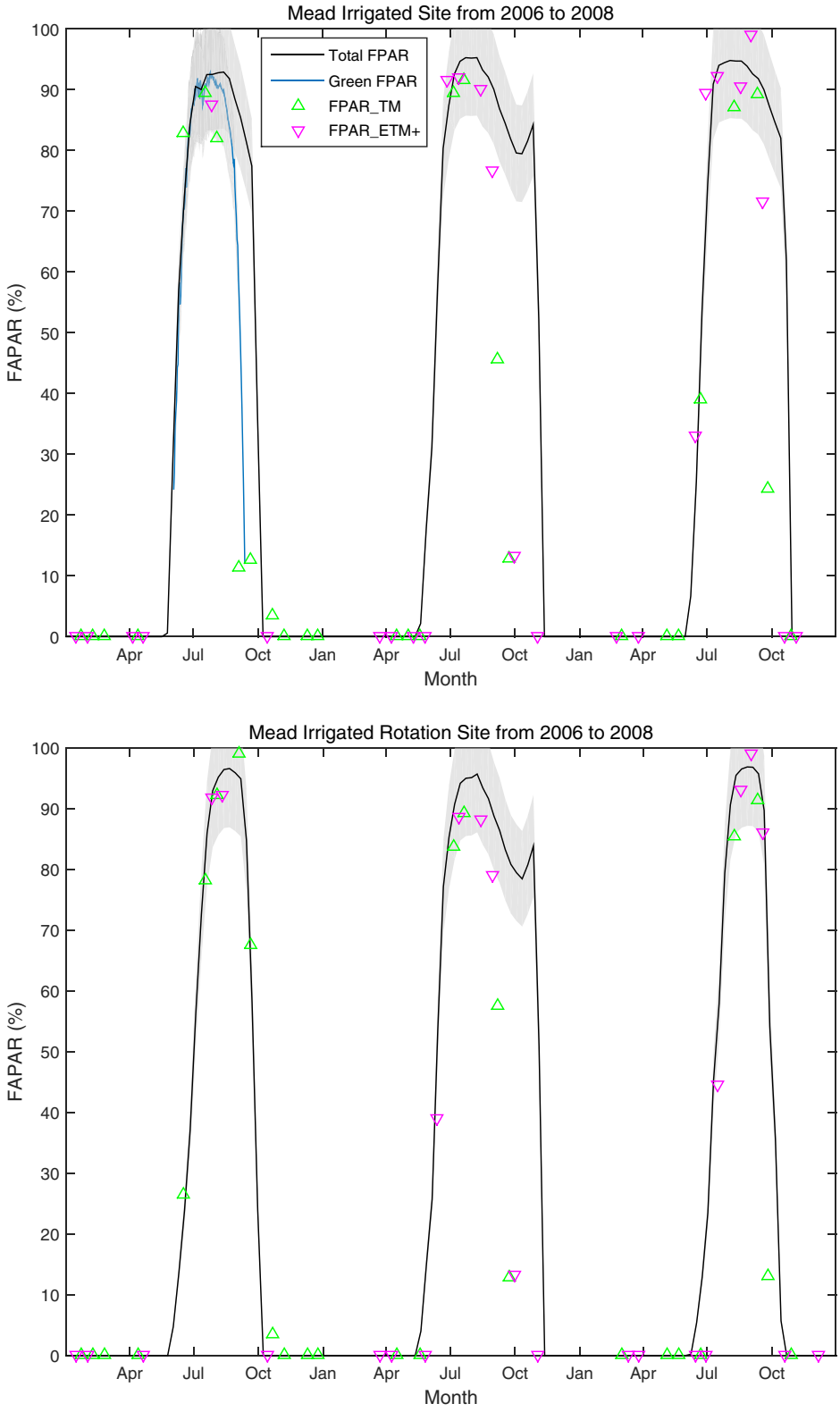

Fig. 10. The time series of in-situ FAPAR measurements and the Landsat FAPAR estimates at four AmeriFlux sites. Green FAPAR measurements are depicted in blue line in the first panel, and total FAPAR measurements are depicted in black line in all panels. The shaded area is the 10% accuracy requirement. The FAPAR estimated from Landsat TM and ETM + surface reflectance are depicted in upward and downward triangles, respectively.

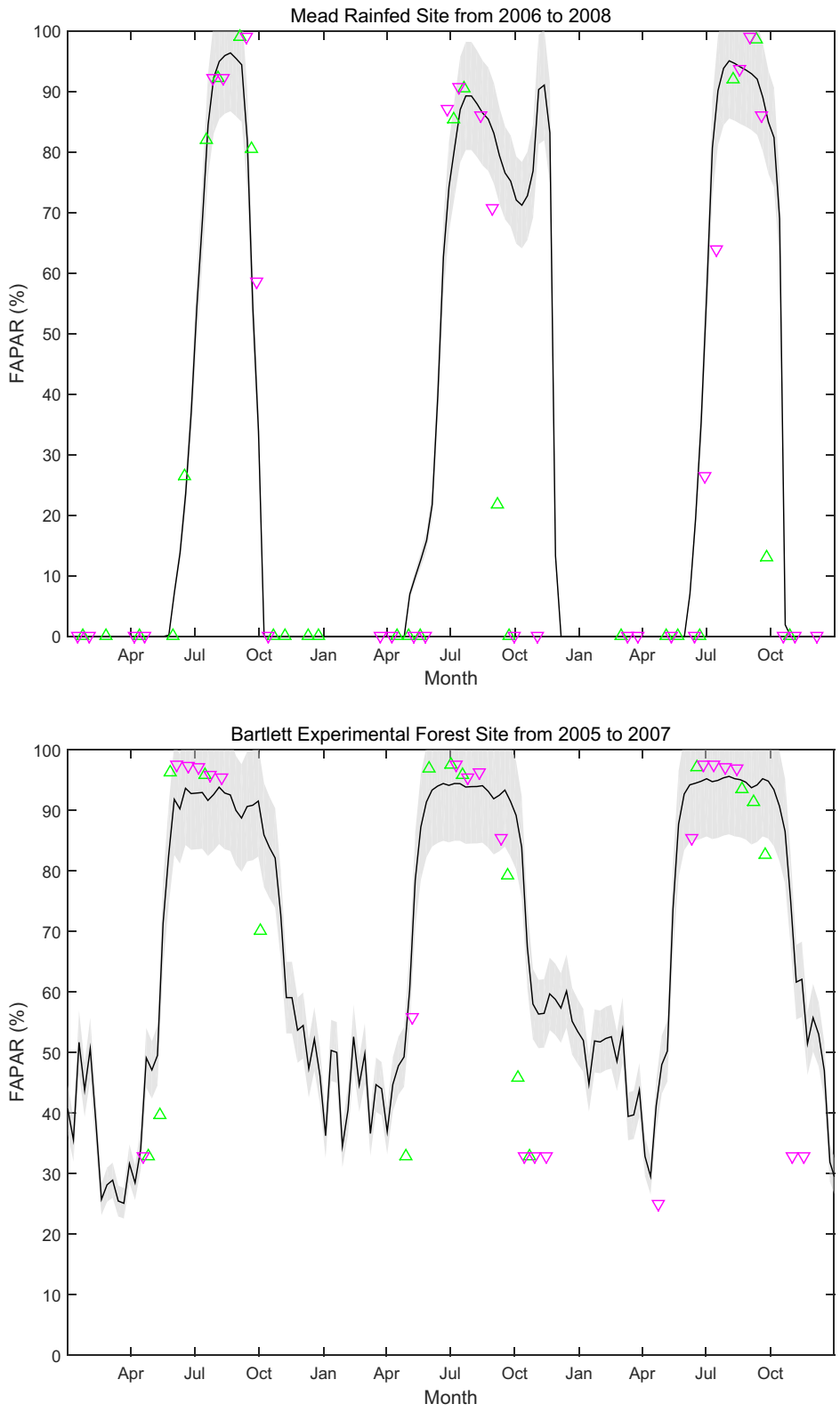

Fig. 10 (*continued*).

0.15) and standard deviation (by 8%) than the MODIS FAPAR product in Case 1, because more pixels with FAPAR values >0.9 are observed in the MISR image than in the MODIS image. The frequency histograms of the MISR and the MODIS FAPAR products agree well in Case 2. The difference between the mean values of the MISR and the MODIS FAPAR products is about 0.05. Overall, the agreements between the FAPAR products differ in the two regions possibly due to the difference in land cover composition.

The frequency histograms of the FAPAR estimates from the Landsat, MODIS, and MISR reflectance images are shown in green, red, and blue

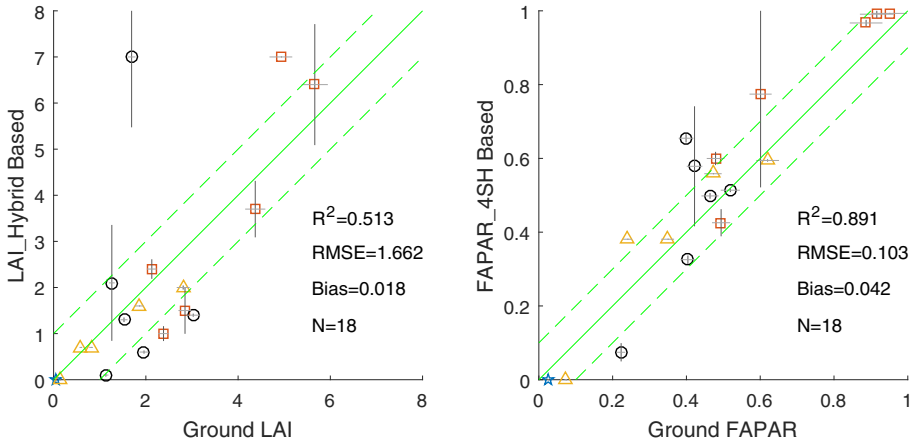

Fig. 11. Validation of the Landsat LAI (left) and FAPAR (right) estimates from this study by using in-situ measurements at VALERI sites. The land cover of shrubland is displayed by a pentagram (*), grass by triangle (Δ), forest by square (□), and crop by circle (○). Horizontal and vertical bars correspond to the uncertainties (±σ). The middle line is $y = x$. The other lines are $y = x \pm 1$ (left) and $y = x \pm 0.1$ (right), respectively.

Table 5
The spatial coverages and imaging dates of the MODIS, MISR and Landsat data used in the two case studies.

Case	MODIS tile	MISR orbit	Landsat orbit	MODIS date	MISR date	Landsat date
Case 1	H10V04	P27B58	P28R31	Aug 5–12, 2006	Aug 4, 2006	Aug 3, 2006
Case 2	H12V04	P12B55	P12R29	Aug 5–12, 2005	Aug 8, 2005	Aug 8, 2005

Case 1 covers three sites: Mead Irrigated, Mead Irrigated Rotation, and Mead Rainfed. Case 2 covers the Bartlett site. The "H" and "V" of MODIS tile means horizontal and vertical, respectively. The "P" and "B" of MISR orbit means path and block, respectively. The "P" and "R" of Landsat orbit means path and row, respectively.

bars in Fig. 14(a) and (c) for Cases 1 and 2, respectively. Generally, the agreements among the Landsat, MODIS, and MISR FAPAR estimates are reasonably good. The mean values of the FAPAR estimates differ within 0.1, and the standard deviations differ within 0.03 for both cases. Therefore, the FAPAR estimates by the presented retrieval model have better performance than the MODIS and MISR products regarding consistency across scales. The comparable results between the estimates from this study and the current products indicate that the retrieval algorithms of FAPAR products can partially justify the differences in their data distributions; thus, the FAPAR values from different satellites agree better when using the same algorithm for retrieval (Seixas et al., 2009). Additionally, this study provides FAPAR estimates at multiple resolutions ranging from 30 m, 500 m, to 1 km, whereas the existing MODIS and MISR FAPAR products are both at 1 km.

6. Discussion and conclusions

This study focuses on developing a new FAPAR model and its parameterizations to achieve an improved accuracy toward the requirement of 0.05. The FAPAR estimates by this model are compared with reference satellite FAPAR products and are validated using a comprehensive set of measurements from two field experiments to meet the requirement for Stage 2 of the validation (Morisette et al., 2006). Intercomparisons and validations are conducted at site and regional scales. The site scale intercomparison and validation results demonstrate that the performances of the MODIS and MISR products vary with land cover types. Generally, the MODIS and the MISR FAPAR products perform well in shrubland and crop sites but are less accurate over grass and forest. This outcome is caused partially by the smaller range of in-situ measured FAPAR values

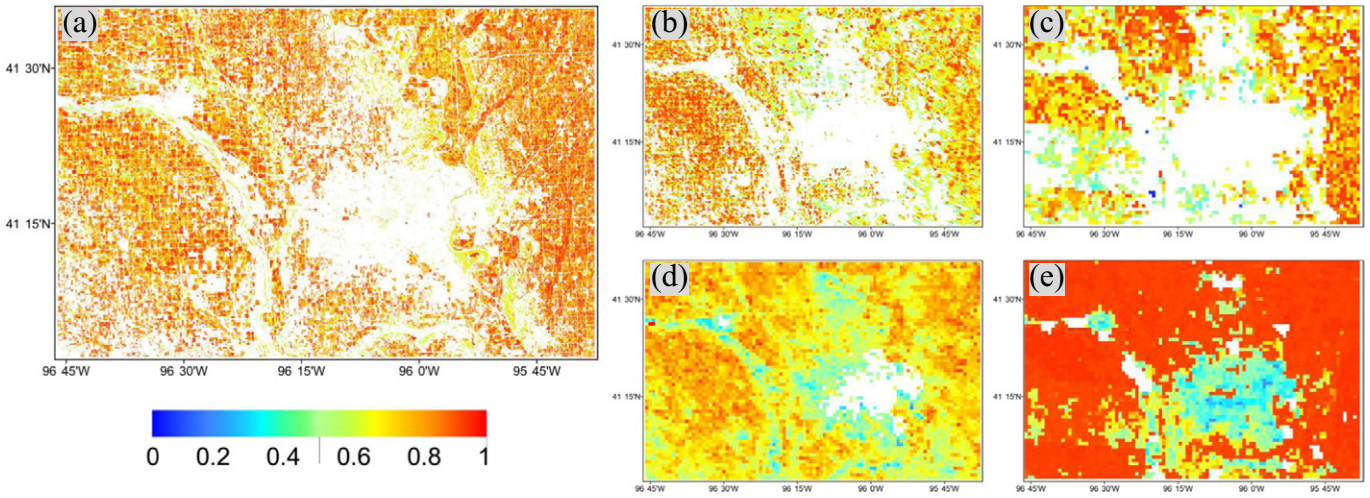

Fig. 12. The FAPAR maps derived from the TM, MODIS, and MISR scenes in the Mead study region in Case 1. (a)–(c) show the TM, MODIS, and MISR FAPAR estimates from this study. (d) and (e) show the MODIS and the MISR FAPAR products.

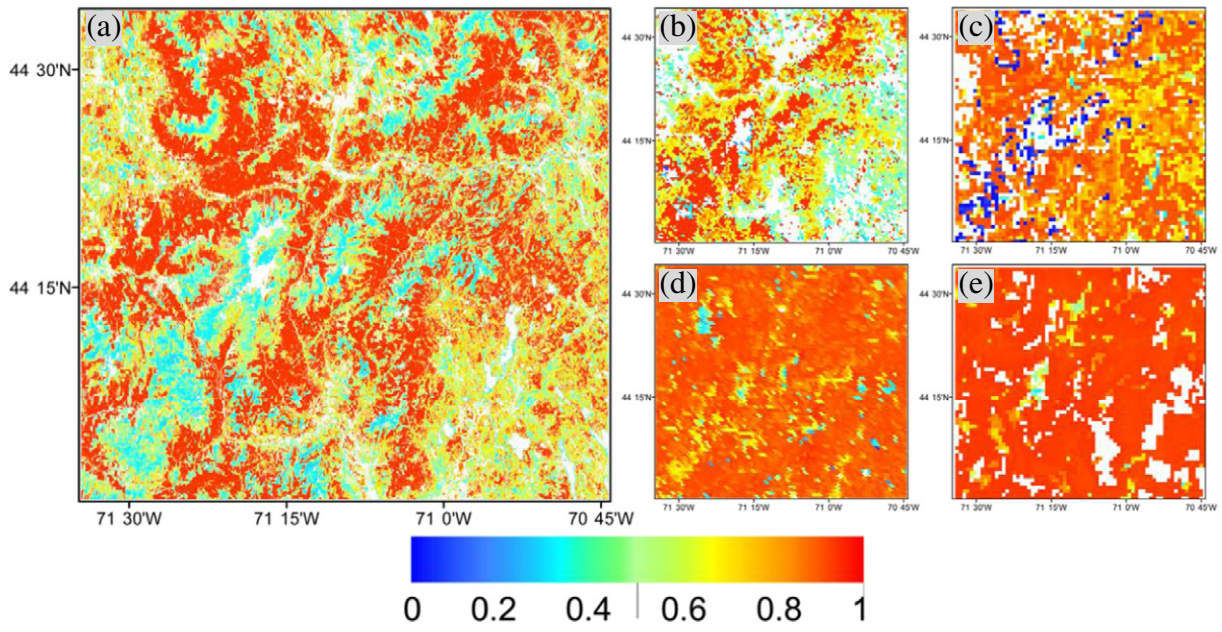

Fig. 13. The FAPAR maps derived from the ETM+, MODIS, and MISR scenes in the Bartlett region in Case 2. (a)–(c) show the ETM+, MODIS, and MISR FAPAR estimates from this study. (d) and (e) show the MODIS and MISR FAPAR products.

over crops and shrubland, at a range of 0.22–0.74 for VALERI sites, compared with larger ranges of FAPAR values over grass and forests, at ranges of 0.07–0.84 and 0.26–0.92, respectively. Larger ranges of FAPAR values allow the FAPAR products to deviate more from the measured values used as truth data here. Additionally, the forests structure includes the understory, tree trunks, branches, and leaves, resulting in complex interactions with photons. Satellite FAPAR products have different assumptions when retrieving FAPAR over forests; thus, their differences are large over forests. These findings resemble the conclusion reported by Pickett-Heaps et al. (2014) such that FAPAR products disagree significantly with in-situ values at forest sites but have relatively high agreements at shrubland and crop sites.

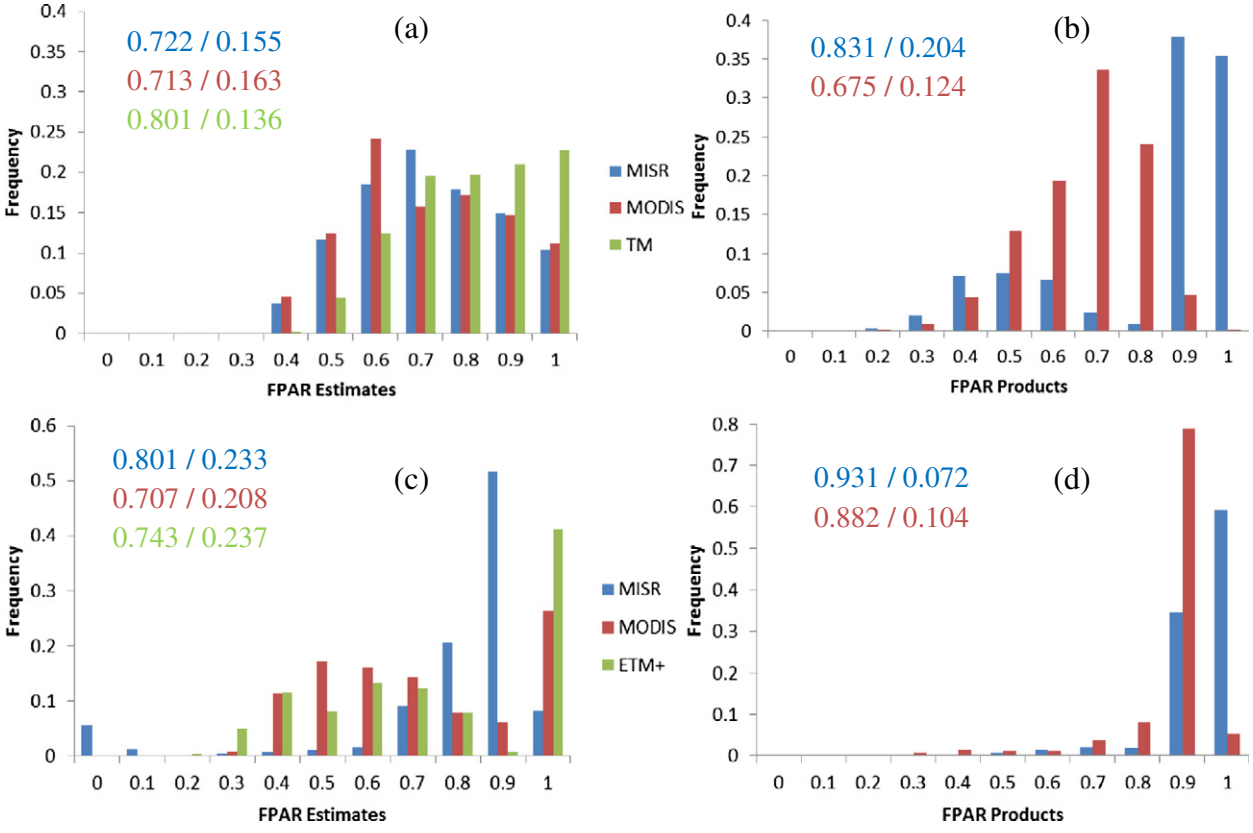

Fig. 14. The FAPAR frequency histograms of the MISR, MODIS, and Landsat scenes in the Mead study region in Case 1 and Case 2. (a) The MISR, MODIS, and ETM+ FAPAR estimates from this study in Case 1. (b) The MISR and MODIS FAPAR products in Case 1. (c) The MISR, MODIS, and ETM+ FAPAR estimates from this study in Case 2. (d) The MISR and MODIS FAPAR products in Case 2. The numbers are the regional mean and standard deviation.

The model from this study has improved the FAPAR accuracy to an average of 0.1. The growing season is successfully identified, and the time series of the FAPAR estimates are smooth over the years. The improvements are apparent at grasslands and forests with a reduction of uncertainty to 0.09, which are attributed to both the new model and the improved inputs. The model presented in this study uses a Nilson parameter λ_0 to account for the vegetation clumping effect, the uncertainty of which could lead to inaccurate FAPAR estimates. Forests and grasses are more homogenous than shrubland and crops with scattered natural vegetation or row crops. Therefore, the empirical values of λ_0 for forests and grasses have lower uncertainty owing to their homogeneity. Thus, the improvements in FAPAR accuracy from this model are more significant for grasses and forests than for shrubland and crops.

The presented model is able to achieve comparable or slightly better performance than the MODIS and the MISR FAPAR models when using the corresponding satellite LAI products as input, as shown in the control experiments. The FAPAR accuracy is further improved when using higher accuracy LAI values as input. Therefore, it is equally essential to develop new FAPAR models and to improve the accuracy of model parameters, particularly LAI, for improving the FAPAR accuracy.

The retrieval rate of the MODIS FAPAR estimates is higher than that of the MISR FAPAR estimates, which is a result of more valid observations in the MODIS than in the MISR surface reflectance data for FAPAR retrieval. Therefore, it is necessary to include the MODIS FAPAR estimates for a long-term and continuous FAPAR time series analysis. However, considering the multi-angular information, the accuracy of the MISR FAPAR estimates is generally better than that of the MODIS FAPAR estimates. The FAPAR estimated from Landsat high spatial resolution data have detailed spatial distribution information; however, Landsat has long revisit time, and the available images are likely to be contaminated by cloud. A data fusion method could potentially be a good solution, integrating the temporal continuity of the MODIS FAPAR estimates, the high accuracy of the MISR FAPAR estimates, and the detailed spatial distribution of the Landsat FAPAR estimates.

Application of the presented model at the regional scale generates consistent FAPAR maps across multiple scales from the Landsat, MODIS, and MISR reflectance data, with a mean difference within 0.1 and a standard deviation difference within 0.03. The MODIS and MISR FAPAR estimates obtained in this study have higher agreements with each other than the MODIS and the MISR FAPAR products in some study regions. Additionally, this study provides FAPAR estimates at three scales of 30 m, 500 m, and 1 km, as a complement to the MODIS and the MISR FAPAR products available at 1 km.

It should be noted that this research has some limitations. Significant efforts must be devoted to reach Stage 3 of the validation. Product accuracy must be thoroughly assessed, and the uncertainties in the product must be well established via independent measurements made in a systematic and statistically robust way that represents global conditions. The presented FAPAR model is suitable for homogeneous landscapes and has better performance over homogeneous land cover. Future study would be focused on developing an advanced FAPAR model to improve accuracy over heterogeneous landscapes.

Acknowledgements

The authors appreciate the help from the ROMC team to deliver results to the system. The authors thank the MODIS land product processing team at Oak Ridge National Laboratory Distributed Active Archive Center for the MODIS Collection 5 data as well as the EOS MISR land processing team (WWW1, WWW2). We are thankful to the NASA LEDAPS project team members for the atmospheric correction preprocessing code (WWW3). The authors thank the Ameriflux and VALERI PIs and staff for publishing the in-situ data (WWW4, WWW5). We would also like to thank the anonymous reviewers for their constructive comments and suggestions. This study was partially funded by the National High-Technology Research and Development Program of China under grant 2013AA122800 and the National Natural Science Foundation of China under grant nos. 41331173.

Appendix A. The parameters for FAPAR estimation

The calculation of FAPAR requires the knowledge of LAI and ϕ, which can be solved by using the following equations:

$$\rho = \rho^1 + \rho^m \tag{A1}$$

where ρ^1 is the contribution of single scattering, expressed as the sum of contributions from illuminated ground, shadow background, illuminated canopy, and shadow canopy.

$$\rho^1 = \rho_g\left\{e^{-\lambda_0\left[\frac{G_S}{\mu_s}+\frac{G_V}{\mu_v}-\frac{G_V}{\mu_v}\Gamma(\phi)\right]LAI} + \left[e^{-\lambda_0\frac{G_V}{\mu_v}LAI} - e^{-\lambda_0\left[\frac{G_S}{\mu_s}+\frac{G_V}{\mu_v}-\frac{G_V}{\mu_v}\Gamma(\phi)\right]LAI}\right]\frac{E_d}{\mu_0 F_0 + E_d}\right\} + \rho_c\left\{\left(1-e^{-\lambda_0\frac{G_V}{\mu_v}LAI\cdot\Gamma(\phi)}\right) + \left[e^{-\lambda_0\frac{G_V}{\mu_v}LAI\cdot\Gamma(\phi)} - e^{-\lambda_0\frac{G_V}{\mu_v}LAI}\right]\frac{E_d}{\mu_0 F_0 + E_d}\right\} \tag{A.2}$$

where E_d is the diffuse irradiance from sky scattering, and $\mu_0 F_0$ is the direct irradiance from solar illumination.

The meanings of other symbols are given in Section 3. The contribution of multi-scattering ρ^m can be expressed by the Hapke model:

$$\rho^m = \frac{\omega}{4}\cdot\frac{1}{\mu_v\mu_0}[H(\mu_v)H(\mu_s)-1]I_{ms} \tag{A3}$$

where ω is single scattering albedo of a single leaf, $\omega \cong 2\rho_v$

$$H\left(\mu_{s,v}\right) = \frac{1+2\mu_{s,v}}{1+2\mu_{s,v}\sqrt{1-\omega}} \tag{A4}$$

$$I_{ms} = \frac{1}{\Delta'}\left(1-e^{-\Delta'\cdot\lambda_0\cdot LAI}\right), \Delta' = \frac{G_s}{\mu_s}+\frac{G_v}{\mu_v} \tag{A5}$$

When solar and viewing directions overlap each other,

$$\rho^m = \rho_v\cdot\frac{\left[H^2(\mu_v)-1\right]}{4\mu_v G_v}\left(1-e^{-2\lambda_0\frac{G_V}{\mu_v}LAI}\right) \tag{A6}$$

Eqs. (A1), (A2), and (A3) express observed reflectance as a function of LAI and ϕ, which can be solved with observations at two or more wavelengths. The equation group is nonlinear and must be solved with an iterative method, an optimization algorithm, or a look up table, the last of which is adopted here, considering its robustness.

References

Asner, G.P., Wessman, C.A., Archer, S., 1998. Scale dependence of absorption of photosynthetically active radiation in terrestrial ecosystems. Ecol. Appl. 8, 1003–1021.

Asrar, G., Myneni, B.J., Choudhury, B.J., 1992. Spatial heterogeneity in vegetation canopies and remote sensing of absorbed photosynthetically active radiation: a modeling study. Remote Sens. Environ. 41, 85–103.

Baret, F., Hagolle, O., Geiger, B., Bicheron, P., Miras, B., Huc, M., Berthelot, B., Nino, F., Weiss, M., Samain, O., Roujean, J.L., Leroy, M., 2007. LAI, fAPAR and fCover CYCLOPES global products derived from VEGETATION - part 1: principles of the algorithm. Remote Sens. Environ. 110, 275–286.

Baret, F., Weiss, M., Lacaze, R., Camacho, F., Makhmara, H., Pacholcyzk, P., Smets, B., 2013. GEOV1: LAI and FAPAR essential climate variables and FCOVER global time series capitalizing over existing products. Part1: principles of development and production. Remote Sens. Environ. 137, 299–309.

Bonan, G.B., Oleson, K.W., Vertenstein, M., Levis, S., Zeng, X., Dai, Y., Dickinson, R.E., Yang, Z.L., 2002. The land surface climatology of the community land model coupled to the NCAR community climate model. J. Clim. 15, 3123–3149.

Camacho, F., Cemicharo, J., Lacaze, R., Baret, F., Weiss, M., 2013. GEOV1: LAI, FAPAR essential climate variables and FCOVER global time series capitalizing over existing products. Part 2: validation and intercomparison with reference products. Remote Sens. Environ. 137, 310–329.

Carrer, D., Roujean, J.L., Lafont, S., Calvet, J.C., Boone, A., Decharme, B., Delire, C., Gastellu-Etchegorry, J.P., 2013. A canopy radiative transfer scheme with explicit FAPAR for the

interactive vegetation model ISBA-A-gs: impact on carbon fluxes. J. Geophys. Res. Biogeosci. 118, 888–903.
Chen, J.M., 1996. Canopy architecture and remote sensing of the fraction of photosynthetically active radiation absorbed by boreal forests. IEEE Trans. Geosci. Remote Sens. 34, 1353–1368.
Fang, H.L., Liang, S.L., McClaran, M.P., van Leeuwen, W.J.D., Drake, S., Marsh, S.E., Thomson, A.M., Izaurralde, R.C., Rosenberg, N.J., 2005. Biophysical characterization and management effects on semiarid rangeland observed from Landsat ETM+ data. IEEE Trans. Geosci. Remote Sens. 43, 125–134.
Fang, H., Wei, S., Liang, S., 2012. Validation of MODIS and CYCLOPES LAI products using global field measurement data. Remote Sens. Environ. 119, 43–54.
Fensholt, R., Sandholt, I., Rasmussen, M.S., 2004. Evaluation of MODIS LAI, fAPAR and the relation between fAPAR and NDVI in a semi-arid environment using in situ measurements. Remote Sens. Environ. 91, 490–507.
Friedl, M.A., 1997. Examining the effects of sensor resolution and sub-pixel heterogeneity on vegetation spectral indices: implications for biophysical modeling. In: Quattrochi, D.A., Goodchild, M.F. (Eds.), Scale in Remote Sensing and GIS. Lewis, Boca Raton, Fla, pp. 113–139.
GCOS, 2011. Systematic Observation Requirements for Satellite-based Data Products for Climate. pp. 79–83.
Gobron, N., Pinty, B., Verstraete, M., Govaerts, Y., 1999. The MERIS Global Vegetation Index (MGVI): description and preliminary application. Int. J. Remote Sens. 20, 1917–1927.
Govaerts, Y.M., Verstraete, M.M., 1998. Raytran: a Monte Carlo ray-tracing model to compute light scattering in three-dimensional heterogeneous media. IEEE Trans. Geosci. Remote Sens. 36, 493–505.
Hall, F., Masek, J.G., Collatz, G.J., 2006. Evaluation of ISLSCP initiative IIFASIR and GIMMS NDVI products and implications for carbon cycle science. J. Geophys. Res.-Atmos. 111. http://dx.doi.org/10.1029/2006JD007438.
Hanan, N.P., Burba, G., Verma, S.B., Berry, J.A., Suyker, A., Walter-Shea, E.A., 2002. Inversion of net ecosystem CO2 flux measurements for estimation of canopy PAR absorption. Glob. Chang. Biol. 8, 563–574.
He, T., Gao, F., Liang, S., Peng, Y., Anderson, M., 2015. Mapping Climatological Bare Soil Albedo during 2000–2012 over the Contiguous United States Using MODIS Data in review.
Houghton, R.A., 1995. Land-use change and the carbon-cycle. Glob. Chang. Biol. 1, 275–287.
Hu, J.N., Tan, B., Shabanov, N., Crean, K.A., Martonchik, J.V., Diner, D.J., Knyazikhin, Y., Myneni, R.B., 2003. Performance of the MISR LAI and FPAR algorithm: a case study in Africa. Remote Sens. Environ. 88, 324–340.
Hu, J.N., Su, Y., Tan, B., Huang, D., Yang, W.Z., Schull, M., Bull, M.A., Martonchik, J.V., Diner, D.J., Knyazikhin, Y., Myneni, R.B., 2007. Analysis of the MISR LA/FPAR product for spatial and temporal coverage, accuracy and consistency. Remote Sens. Environ. 107, 334–347.
Huemmrich, K.F., Privette, J.L., Mukelabai, M., Myneni, R.B., Knyazikhin, Y., 2005. Time-series validation of MODIS land biophysical products in a Kalahari woodland, Africa. Int. J. Remote Sens. 26, 4381–4398.
Kaminski, T., Knorr, W., Scholze, M., Gobron, N., Pinty, B., Giering, R., Mathieu, P.P., 2012. Consistent assimilation of MERIS FAPAR and atmospheric CO2 into a terrestrial vegetation model and interactive mission benefit analysis. Biogeosciences 9, 3173–3184.
Kanniah, K.D., Beringer, J., Hutley, L.B., Tapper, N.J., Zhu, X., 2009. Evaluation of collections 4 and 5 of the MODIS gross primary productivity product and algorithm improvement at a tropical savanna site in northern Australia. Remote Sens. Environ. 113, 1808–1822.
Knyazikhin, Y., Martonchik, J.V., Diner, D.J., Myneni, R.B., Verstraete, M., Pinty, B., Gobron, N., 1998a. Estimation of vegetation canopy leaf area index and fraction of absorbed photosynthetically active radiation from atmosphere-corrected MISR data. J. Geophys. Res.-Atmos. 103, 32239–32256.
Knyazikhin, Y., Martonchik, J.V., Myneni, R.B., Diner, D.J., Running, S.W., 1998b. Synergistic algorithm for estimating vegetation canopy leaf area index and fraction of absorbed photosynthetically active radiation from MODIS and MISR data. J. Geophys. Res.-Atmos. 103, 32257–32275.
Li, Z.Q., Whitlock, C.H., Charlock, T.P., 1995. Assessment of the global monthly mean surface insolation estimated from satellite measurements using global energy-balance archive data. J. Clim. 8, 315–328.
Liang, S., 2004. Quantitative Remote Sensing of Land Surfaces. John Wiley & Sons, Inc., New York.
Liang, S.L., 2007. Recent developments in estimating land surface biogeophysical variables from optical remote sensing. Prog. Phys. Geogr. 31, 501–516.
Liang, S., Li, X., Wang, J., 2012. Advanced Remote Sensing: Terrestrial Information Extraction and Applications. Academic Press, 2012 ISBN 9780123859556.
Martinez, B., Camacho, F., Verger, A., Garcia-Haro, F.J., Gilabert, M.A., 2013. Intercomparison and quality assessment of MERIS, MODIS and SEVIRI FAPAR products over the Iberian Peninsula. Int. J. Appl. Earth Obs. Geoinf. 21, 463–476.
Masek, J.G., Vermote, E.F., Saleous, N.E., Wolfe, R., Hall, F.G., Huemmrich, K.F., Gao, F., Kutler, J., Lim, T.K., 2006. A Landsat surface reflectance dataset for North America, 1990–2000. IEEE Geosci. Remote Sens. Lett. 3, 68–72.
Maselli, F., Chiesi, M., Fibbi, L., Moriondo, M., 2008. Integration of remote sensing and ecosystem modelling techniques to estimate forest net carbon uptake. Int. J. Remote Sens. 29, 2437–2443.
McCallum, A., Wagner, W., Schmullius, C., Shvidenko, A., Obersteiner, M., Fritz, S., Nilsson, S., 2010. Comparison of four global FAPAR datasets over Northern Eurasia for the year 2000. Remote Sens. Environ. 114, 941–949.
Morisette, J.T., Baret, F., Privette, J.L., Myneni, R.B., Nickeson, J.E., Garrigues, S., Shabanov, N.V., Weiss, M., Fernandes, R.A., Leblanc, S.G., Kalacska, M., Sanchez-Azofeifa, G.A., Chubey, M., Rivard, B., Stenberg, P., Rautiainen, M., Voipio, P., Manninen, T., Pilant, A.N., Lewis, T.E., Iiames, J.S., Colombo, R., Meroni, M., Busetto, L., Cohen, W.B., Turner, D.P., Warner, E.D., Petersen, G.W., Seufert, G., Cook, R., 2006. Validation of global moderate-resolution LAI products: a framework proposed within the CEOS Land Product Validation subgroup. IEEE Trans. Geosci. Remote Sens. 44, 1804–1817.
Myneni, R.B., Hoffman, S., Knyazikhin, Y., Privette, J.L., Glassy, J., Tian, Y., Wang, Y., Song, X., Zhang, Y., Smith, G.R., Lotsch, A., Friedl, M., Morisette, J.T., Votava, P., Nemani, R.R., Running, S.W., 2002. Global products of vegetation leaf area and fraction absorbed PAR from year one of MODIS data. Remote Sens. Environ. 83, 214–231.
Olofsson, P., Eklundh, L., 2007. Estimation of absorbed PAR across Scandinavia from satellite measurements. Part II: modeling and evaluating the fractional absorption. Remote Sens. Environ. 110, 240–251.
Pickett-Heaps, C.A., Canadell, J.G., Briggs, P.R., Gobron, N., Haverd, V., Paget, M.J., Pinty, B., Raupach, M.R., 2014. Evaluation of six satellite-derived Fraction of Absorbed Photosynthetic Active Radiation (FAPAR) products across the Australian continent. Remote Sens. Environ. 140, 241–256.
Pinty, B., Clerici, M., Andredakis, I., Kaminski, T., Taberner, M., Verstraete, M.M., Gobron, N., Plummer, S., Widlowski, J.L., 2011. Exploiting the MODIS albedos with the Two-stream Inversion Package (JRC-TIP): 2. Fractions of transmitted and absorbed fluxes in the vegetation and soil layers. J. Geophys. Res.-Atmos. 116.
Ross, J., 1981. The Radiation Regime and Architecture of Plant Stands. Dr. W. Junk Publishers, The Hague, Boston and London.
Seixas, J., Carvalhais, N., Nunes, C., Benali, A., 2009. Comparative analysis of MODIS-FAPAR and MERIS-MGVI datasets: Potential impacts on ecosystem modeling. Remote Sens. Environ. 113, 2547–2559.
Sellers, P.J., Dickinson, R.E., Randall, D.A., Betts, A.K., Hall, F.G., Berry, J.A., Collatz, G.J., Denning, A.S., Mooney, H.A., Nobre, C.A., Sato, N., Field, C.B., Henderson-Sellers, A., 1997. Modeling the exchanges of energy, water, and carbon between continents and the atmosphere. Science 275, 502–509.
Serbin, S.P., Ahl, D.E., Gower, S.T., 2013. Spatial and temporal validation of the MODIS LAI and FPAR products across a boreal forest wildfire chronosequence. Remote Sens. Environ. 133, 71–84.
Shabanov, N.V., Huang, D., Yang, W.Z., Tan, B., Knyazikhin, Y., Myneni, R.B., Ahl, D.E., Gower, S.T., Huete, A.R., Aragao, L., Shimabukuro, Y.E., 2005. Analysis and optimization of the MODIS leaf area index algorithm retrievals over broadleaf forests. IEEE Trans. Geosci. Remote Sens. 43, 1855–1865.
Steinberg, D.C., Goetz, S.J., Hyer, E.J., 2006. Validation of MODIS F-PAR products in boreal forests of Alaska. IEEE Trans. Geosci. Remote Sens. 44, 1818–1828.
Tao, X., Yan, B., Wang, K., Wu, D., Fan, W., Xu, X., Liang, S., 2009. Scale transformation of leaf area index product retrieved from multi-resolution remotely sensed data: Analysis and case studies. Int. J. Remote Sens. 30, 5383–5395.
Tao, X., Liang, S.L., He, T., 2013. Estimation of fraction of absorbed photosynthetically active radiation from multiple satellite data. 2013 Ieee International Geoscience and Remote Sensing Symposium (pp. 3072–3075). Ieee, New York.
Tao, X., Liang, S., Wang, D.D., 2015. Assessment of five global satellite products of fraction of absorbed photosynthetically active radiation: intercomparison and direct validation against ground-based data. Remote Sens. Environ. 163, 270–285.
Tian, Y., Dickinson, R.E., Zhou, L., Zeng, X., Dai, Y., Myneni, R.B., Knyazikhin, Y., Zhang, X., Friedl, M., Yu, I.I., Wu, W., Shaikh, M., 2004. Comparison of seasonal and spatial variations of leaf area index and fraction of absorbed photosynthetically active radiation from Moderate Resolution Imaging Spectroradiometer (MODIS) and Common Land Model. J. Geophys. Res.-Atmos. 109. http://dx.doi.org/10.1029/2003JD003777.
Turner, D.P., Ritts, W.D., Cohen, W.B., Maeirsperger, T.K., Gower, S.T., Kirschbaum, A.A., Running, S.W., Zhao, M.S., Wofsy, S.C., Dunn, A.L., Law, B.E., Campbell, J.L., Oechel, W.C., Kwon, H.J., Meyers, T.P., Small, E.E., Kurc, S.A., Gamon, J.A., 2005. Site-level evaluation of satellite-based global terrestrial gross primary production and net primary production monitoring. Glob. Chang. Biol. 11, 666–684.
Vina, A., Gitelson, A.A., 2005. New developments in the remote estimation of the fraction of absorbed photosynthetically active radiation in crops. Geophys. Res. Lett. 32.
Weiss, M., Baret, F., Garrigues, S., Lacaze, R., 2007. LAI and fAPAR CYCLOPES global products derived from VEGETATION. Part 2: validation and comparison with MODIS collection 4 products. Remote Sens. Environ. 110, 317–331.
Widlowski, J.L., 2010. On the bias of instantaneous FAPAR estimates in open-canopy forests. Agric. For. Meteorol. 150, 1501–1522.
Widlowski, J.L., Taberner, M., Pinty, B., Bruniquel-Pinel, V., Disney, M., Fernandes, R., Gastellu-Etchegorry, J.P., Gobron, N., Kuusk, A., Lavergne, T., Leblanc, S., Lewis, P.E., Martin, E., Mottus, M., North, P.R.J., Qin, W., Robustelli, M., Rochdi, N., Ruiloba, R., Soler, C., Thompson, R., Verhoef, W., Verstraete, M.M., Xie, D., 2007. Third Radiation Transfer Model Intercomparison (RAMI) exercise: documenting progress in canopy reflectance models. J. Geophys. Res.-Atmos. 112 Art. No. D09111.
Widlowski, J.L., Robustelli, M., Disney, M., Gastellu-Etchegorry, J.P., Lavergne, T., Lewis, P., North, P.R.J., Pinty, B., Thompson, R., Verstraete, M.M., 2008. The RAMI On-line Model Checker (ROMC): a web-based benchmarking facility for canopy reflectance models. Remote Sens. Environ. 112, 1144–1150.
Widlowski, J.L., Pinty, B., Clerici, M., Dai, Y., De Kauwe, M., de Ridder, K., Kallel, A., Kobayashi, H., Lavergne, T., Ni-Meister, W., Olchev, A., Quaife, T., Wang, S., Yang, W., Yang, Y., Yuan, H., 2011. RAMI4PILPS: An intercomparison of formulations for the partitioning of solar radiation in land surface models. J. Geophys. Res. Biogeosci. 116.
WWW1, d. The MODIS Collection 5 datahttp://ladsweb.nascom.nasa.gov/data/search.html.
WWW2, d. The MISR datahttp://l0dup05.larc.nasa.gov/MISR/cgi-bin/MISR/main.cgi.
WWW3, d. The Landsat TM and ETM+ datahttp://espa.cr.usgs.gov.
WWW4, d. The VALERI validation datahttp://w3.avignon.inra.fr/valeri/fic_htm/database/main.php.
WWW5, d. The AmeriFlux validation datahttp://ameriflux.ornl.gov.
WWW6, d. The RAMI Online Model Checkerhttp://romc.jrc.ec.europa.eu.

Xiao, Z.Q., Liang, S.L., Sun, R., Wang, J.D., Jiang, B., 2015a. Estimating the fraction of absorbed photosynthetically active radiation from the MODIS data based GLASS leaf area index product. Remote Sens. Environ. 171, 105–117.

Xiao, Z.Q., Liang, S.L., Wang, J.D., Xie, D.H., Song, J.L., Fensholt, R., 2015b. A framework for consistent estimation of leaf area index, fraction of absorbed photosynthetically active radiation, and surface albedo from MODIS time-series data. IEEE Trans. Geosci. Remote Sens. 53, 3178–3197.

Xu, X., Fan, W., Tao, X., 2009. The spatial scaling effect of continuous canopy leaves area index retrieved by remote sensing. Sci. China Ser. D Earth Sci. 52, 393–401.

Yang, W.Z., Huang, D., Tan, B., Stroeve, J.C., Shabanov, N.V., Knyazikhin, Y., Nemani, R.R., Myneni, R.B., 2006. Analysis of leaf area index and fraction of PAR absorbed by vegetation products from the terra MODIS sensor: 2000–2005. IEEE Trans. Geosci. Remote Sens. 44, 1829–1842.

Zhang, Q., Xiao, X., Braswell, B., Linder, E., Baret, F., Moore III, B., 2005. Estimating light absorption by chlorophyll, leaf and canopy in a deciduous broadleaf forest using MODIS data and a radiative transfer model. Remote Sens. Environ. 99, 357–371.